Struct Multidisc Optim (2018) 57:161–182
DOI 10.1007/s00158-017-1768-3

RESEARCH PAPER

# Multi-material topology optimization with multiple volume constraints: a general approach applied to ground structures with material nonlinearity

**Xiaojia Shelly Zhang**[1] · **Glaucio H. Paulino**[1] · **Adeildo S. Ramos Jr.**[2]

Received: 17 January 2017 / Revised: 19 May 2017 / Accepted: 12 June 2017 / Published online: 6 September 2017


**Abstract** Multi-material topology optimization is a practical tool that allows for improved structural designs. However, most studies are presented in the context of continuum topology optimization – few studies focus on truss topology optimization. Moreover, most work in this field has been restricted to linear material behavior with limited volume constraint settings for multiple materials. To address these issues, we propose an efficient multi-material topology optimization formulation considering material nonlinearity. The proposed formulation handles an arbitrary number of candidate materials with flexible material properties, features freely specified material layers, and includes a generalized volume constraint setting. To efficiently handle such arbitrary volume constraints, we derive a design update scheme that performs robust updates of the design variables associated with each volume constraint independently. The derivation is based on the separable feature of the dual problem of the convex approximated primal subproblem with respect to the Lagrange multipliers, and thus the update of design variables in each volume constraint only depends on the corresponding Lagrange multiplier. Through examples in 2D and 3D, using combinations of Ogden-based, bilinear, and linear materials, we demonstrate that the proposed multi-material topology optimization framework with the presented update scheme leads to a design tool that not only finds the optimal topology but also selects the proper type and amount of material. The design update scheme is named ZPR (phonetically, zipper), after the initials of the authors' last names (Zhang-Paulino-Ramos Jr.).

**Keywords** Multi-material topology optimization · Multiple volume constraints · ZPR update scheme · Ground structure method · Material nonlinearity · Design update scheme · Potential energy · Discrete filter · Multiple load cases · KKT conditions

✉ Glaucio H. Paulino
paulino@gatech.edu

Xiaojia Shelly Zhang
xzhang645@gatech.edu

Adeildo S. Ramos Jr.
adramos@lccv.ufal.br

[1] School of Civil and Environmental Engineering, Georgia Institute of Technology, 790 Atlantic Drive NW, Atlanta, GA 30332-0355, USA

[2] Laboratory of Scientific Computing and Visualization Technology Center, Federal University of Alagoas, Maceió, AL 57092-970, Brazil

## 1 Introduction

Topology optimization is a powerful computational design tool used to find optimal layouts of structures and material microstructures. Within the field of topology optimization, multi-material topology optimization is an emerging trend because practical engineering designs, such as buildings, aircraft, and composite materials typically consist of multiple material types. The literature on multi-material topology optimization is vast and growing but mostly focuses on the continuum setting. With the density-based approach, various generalizations and extensions of the Solid Isotropic Material with Penalization (SIMP) (Bendsøe and Sigmund 1999) or other material interpolation schemes for single-material topology optimization are made to accommodate multiple materials. For example, Sigmund and Torquato (1997) and Gibiansky and Sigmund (2000) present extensions of the SIMP model to

three-phase materials (two material phases plus one void phase) and apply them to the design of material microstructures with extreme thermal expansion and extreme bulk moduli. Hvejsel and Lund (2011) generalize the SIMP scheme and the Rational Approximation of Material Properties (RAMP) scheme (Stolpe and Svanberg 2001) to include an arbitrary number of material phases. However, in order to enforce the selection of, at most or exactly, one material at each design subdomain, their study uses a large number of sparse linear constraints. A similar generalization of the SIMP scheme that includes an arbitrary number of material phases is made by Stegmann and Lund (2005), who use the Discrete Material Optimization (DMO) in the design of laminated composite structures. Another variation of the scheme by Yin and Ananthasuresh (2001) proposes a peak function approach that uses only one density variable to interpolate the effective material properties as opposed to multiple density variables. Their scheme uses a Gaussian distribution "peak function" as the weight of each material phase, and the selection of a given material phase is made if the density variable corresponds to a material peak. In addition to the density-based approach, phase-field (Wallin et al. 2015; Zhou and Wang 2007; Tavakoli and Mohseni 2014) and level set (Wang and Wang 2004; 2005; Wang et al. 2005; Mei and Wang 2004) approaches have also been used for multi-material topology optimization formulations.

While the majority of existing studies of multi-material topology optimization deals with the continuum setting, only a small number of studies in multi-material topology optimization include discrete elements, e.g., truss and lattice networks. Among these studies, Stanković et al. (2015) propose a multi-material formulation to optimize lattice structures, incorporating manufacturing constraints. Their study uses the Young's modulus of each truss as the design variables and optimizes them on a layout with fixed cross-sectional areas. Other studies have attempted to integrate truss elements into continuum topology optimization by considering concrete as a continuum solid and steel rebars as truss members (see, e.g., Gaynor et al. (2012), Victoria et al. (2011), Bogomolny and Amir (2012), Amir and Sigmund (2013), and Zegard and Paulino (2013)) for the purpose of designing reinforced concrete structures and studying strut and tie models. However, in the literature, few multi-material topology optimization studies focus on truss layout optimization, which is the emphasis of our work.

A promising technique to optimize truss layouts is the ground structure method (GSM), see, e.g., Dorn et al. (1964), Kirsch (1989), Kirsch (1993), Rozvany et al. (1995), Christensen and Klarbring (2009), and Bendsøe and Sigmund (2003). In this technique, the design domain is discretized by a set of nodes, which are interconnected by truss members to form an initial ground structure (GS). By means of an update scheme and sensitivity information, the final design is then obtained by gradually removing unnecessary members from the initial GS (subtractive method).

*For the initial assignment of material layers in the GSM in the present paper, each candidate material is associated with a design layer (ground structure); thus, users are free to specify the location of each material. The multiple material layers can either share or split the design domain, or combine both, as demonstrated in* Fig. 1. *Scenario* 1 *(*Fig. 1c*) shows the case where the initial ground structures associated with the four materials are overlapping and is designed to enable automatic assignment of the materials. Scenario 2 (*Fig. 1d*) can be used to fulfill various design requirements such as assigning certain materials in specific locations of a structure. As shown in* Fig. 1e*, sharing & splitting can be combined to enable a more flexible design space.*

One limitation of most existing work in multi-material topology optimization is that only linear material behavior is considered (for the study that considers nonlinear material behavior, see Wallin et al. (2015) for multi-material phase-field topology optimization under finite deformation). However, real materials generally display nonlinear constitutive relations. Studies of material nonlinearity in single material topology optimization (e.g., Achtziger (1996), Ohsaki (2010), Sokół (2011), Ramos and Paulino (2015), and Zhang et al. (2017)) have demonstrated the impact of accounting for nonlinear material behavior in structural optimization. For instance, it has been shown that various optimal topologies can be obtained in material nonlinear cases by changing the material behavior and load level. In the case of multiple materials with linear material behavior, an individual volume constraint has to be assigned to each candidate material to ensure its presence in the optimized topology. If one total/global volume constraint is assigned to all the linear candidate materials, the optimizer always favors the best linear candidate material, e.g. the stiffest material in the minimum compliance optimization, and final topologies consisting of only a single material type can occur, as shown in Fig. 2b. However, if the nonlinear material behavior is incorporated in multi-material topology optimization, the optimizer naturally avoids consistently favoring the stiffest linear material and, therefore, enables a more general setting of volume constraints. As demonstrated in Fig. 2c, when a global volume constraint is assigned to two nonlinear candidate materials (one tension-dominated and the other compression-dominated), the resulting topology contains both nonlinear candidate materials. To address the aforementioned issues, we incorporate material nonlinearity into multi-material optimization because it produces various optimized structures and enables enhanced freedom of volume constraints.

From the optimization formulation perspective, another limitation of multi-material topology optimization is related

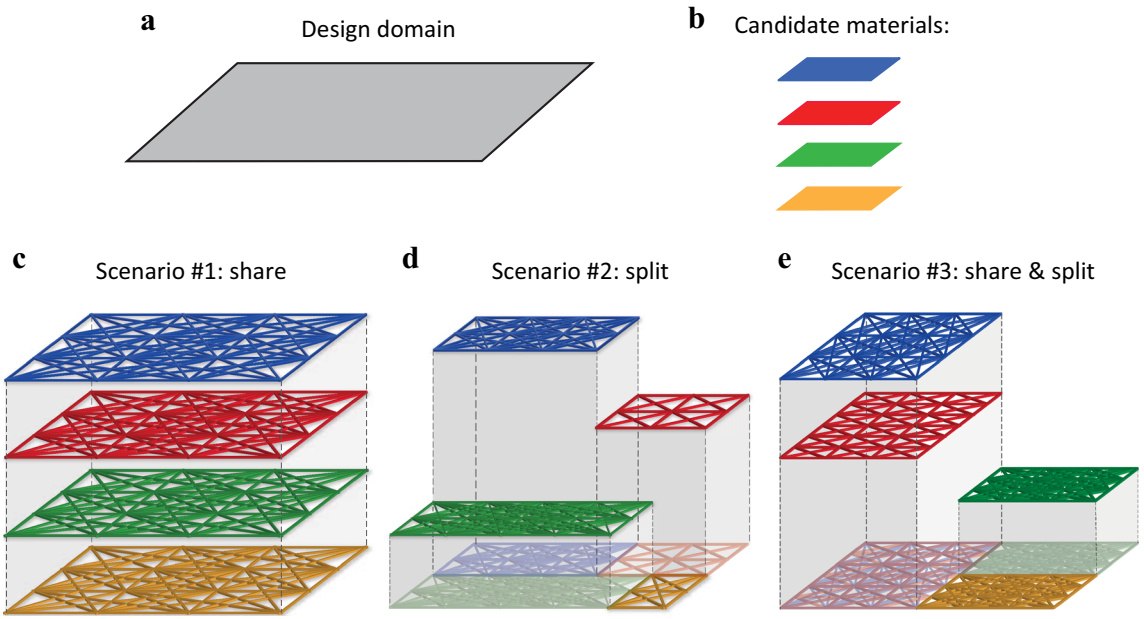


**Fig. 1** Illustration of the combinations of material layers: **a** Design domain; **b** candidate materials; **c** Scenario #1, four materials share the domain (initial ground structures of all materials overlap) enabling automatic material assignment; **d** Scenario #2, four materials split the domain, which can be used to fulfill certain design needs; **e** Scenario #3, four materials share & split the domain, which enables a more flexible design space. (Online version in color)

to the limited settings of volume constraints and the subsequent need for a tailored update scheme. Most studies on multi-material topology optimization either use a total/global volume constraint for all materials (e.g., Hvejsel and Lund (2011), Yin and Ananthasuresh (2001), Gaynor et al. (2012), Victoria et al. (2011), Bogomolny and Amir (2012), and Amir and Sigmund (2013)), which may lead to issues with linear materials (see Fig. 2b); or assign an individual volume constraint to each material (e.g., Sigmund and Torquato (1997), Gibiansky and Sigmund (2000), Wallin et al. (2015), Zhou and Wang (2007), Tavakoli and Mohseni (2014), Wang and Wang (2004), and Wang et al. (2005)), which may impose higher demands on computational implementations and update schemes. A more general setting, e.g., the combination of both types of constraints for various design scenarios, is rarely considered. In an effort to enable a more general setting of the volume constraints for multi-material topology optimization, an update scheme that handles multiple constraints is naturally needed. Although the Optimality Criteria (OC) method is a robust update scheme for single material topology optimization (see, for example, Christensen and Klarbring 2009; Groenwold and Etman 2008), it generally deals with one constraint, and thus, cannot be directly applied into multi-material topology optimization. An OC method that handles multiple constraints is discussed in Haftka and Gürdal (1992), and an extension of the OC method to handle multiple displacement constraints is presented in Yin and Yang (2001); both methods require the calculation of coupled Lagrange multipliers. On the other hand, the multi-material topology optimization literature typically adopts general-purpose update schemes, such as sequential linear programming (Sigmund and Torquato 1997) or the Method of Moving Asymptotes (MMA) (Svanberg 1987). An active-phase algorithm that extends the OC method for multi-material topology optimization is proposed by Tavakoli and Mohseni (2014). Similar to the Gauss-Seidel and Jacobi iterative optimization methods, the active-phase algorithm arranges the material phases by stiffness and performs sequential binary updates using the OC method. This active-phase algorithm is further studied in the work of Cui and Chen (2014) and Park and Sutradhar (2015) with improved performance. However, the active-phase algorithm only applies to linear material behavior and loses efficiency as the number of candidate materials increases. When nonlinear material behavior is considered in multi-material topology optimization, the sequential binary updates of the active-phase algorithm become challenging with respect to arranging a pre-defined ordering scheme for nonlinear candidate materials. *Therefore, an effective and efficient update method, tailored for multi-material topology optimization with an arbitrary number of volume constraints and capable of handling general nonlinear material behavior, is needed.*

*Taking into account the aforementioned limitations, we propose an efficient multi-material optimization formulation. This formulation incorporates nonlinear material behavior and is designed to account for an arbitrary number*

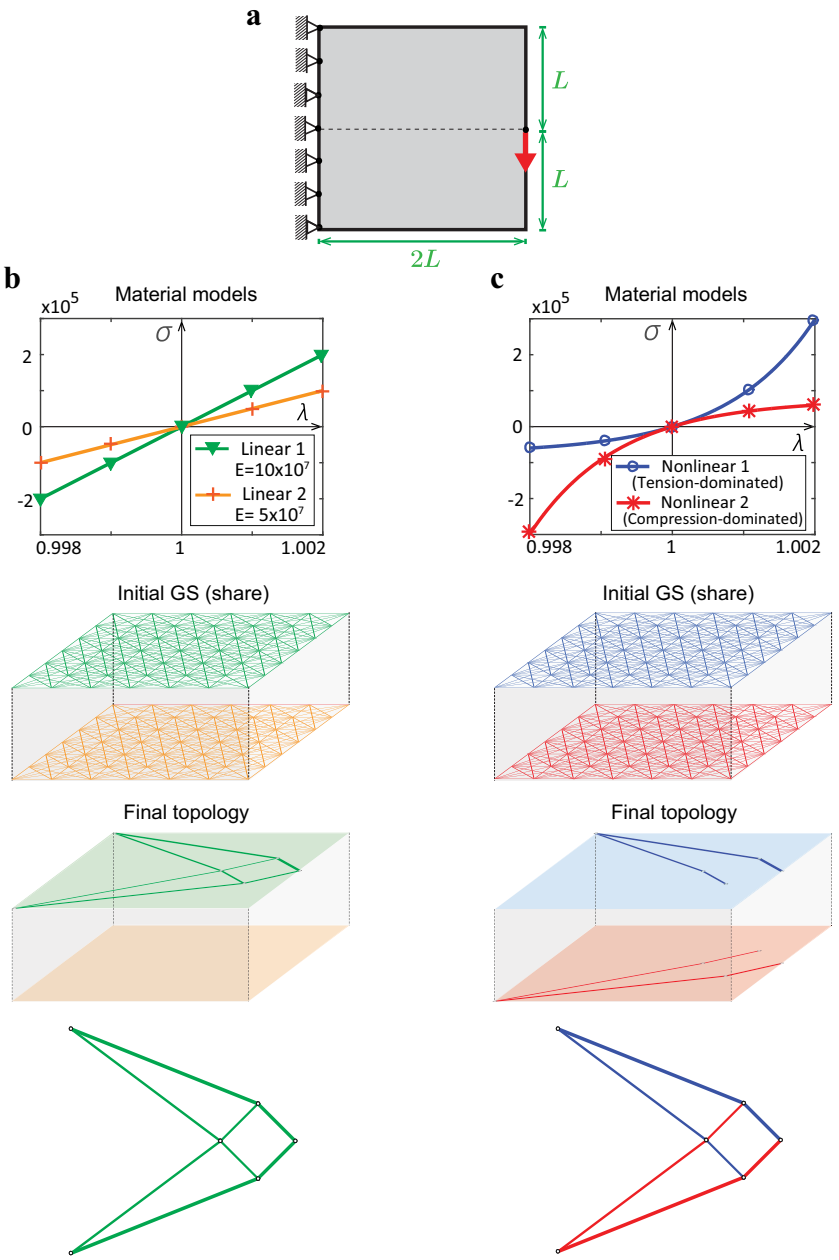


**Fig. 2** Multi-material topology optimization (with one total/global volume constraint): Linear versus nonlinear materials. **a** Design domain; **b** two linear material models, initial material distribution (schematic GSs), and the corresponding optimized structure that favors the stiffer linear material; **c** two nonlinear Ogden-based material models, initial material distribution (schematic GSs), and the corresponding optimized structure that contains both nonlinear materials. (Online version in color)

*of candidate materials with general scenarios of volume constraints. In this study, we present a design update scheme, called ZPR (Zhang-Paulino-Ramos Jr.), that is capable of handling an arbitrary number of volume constraints. This tailored update scheme performs efficient and robust updates of the design variables associated with each volume constraint (in an independent fashion).*

The remainder of the paper is organized as follows. Section 2 proposes the multi-material topology optimization formulation using the GSM, followed by sensitivity analysis, Karush-Kuhn-Tucker (KKT) conditions, incorporation of a discrete filter, and remarks of the proposed formulation. Section 3 presents the ZPR design update scheme and is followed by its detailed derivation. Section 4 describes selected material nonlinear models and their corresponding strain energy density functions. Section 5 presents numerical examples in two- and three-dimensions, highlighting the properties of the proposed formulation, and Section 6 provides concluding remarks with suggestions for expanding our work.

## 2 Multi-material topology optimization

This section introduces the proposed formulation of multi-material topology optimization using the GSM, its

sensitivity analysis, the KKT conditions, and the incorporation of the discrete filter. We further provide some remarks on the proposed formulation.

### 2.1 Formulation

First, we present the proposed multi-material topology optimization formulation for trusses with the assumption of small deformation. The topology design consists of determining the cross-sectional areas of the truss members using the GSM. Assuming a total of $m$ types of materials, we denote $\boldsymbol{x}_i$ as the design variables (cross-sectional areas of the truss elements) associated with material $i$, where $i = 1, ..., m$ are the material indices. We also assume a total of $nc$ independent volume constraints, where $1 \leq nc \leq m$, and denote $\mathscr{G}^j$ as the set of material indices associated with the $j$th volume constraint. The proposed formulation of multi-material topology optimization using the GSM is given as

$$\begin{aligned}
\min_{\boldsymbol{x}_1,...,\boldsymbol{x}_m} \quad & J(\boldsymbol{x}_1, ..., \boldsymbol{x}_m) = \min_{\boldsymbol{x}_1,...,\boldsymbol{x}_m} -\Pi(\boldsymbol{x}_1, ..., \boldsymbol{x}_m, \boldsymbol{u}(\boldsymbol{x}_1, ..., \boldsymbol{x}_m)) \\
\text{s.t.} \quad & g^j(\boldsymbol{x}_1, ..., \boldsymbol{x}_m) = \sum_{i \in \mathscr{G}^j} \boldsymbol{L}_i^{\mathrm{T}} \boldsymbol{x}_i - V_{\max}^j \leq 0, \quad j = 1, ..., nc, \\
& x_{\min} \leq x_i^{(e)} \leq x_{\max}, \ i = 1, ..., m, \ \text{and } e = 1, ..., M_i, \\
\text{with} \quad & \boldsymbol{u}(\boldsymbol{x}_1, ..., \boldsymbol{x}_m) = \arg\min_{\boldsymbol{u}} \Pi(\boldsymbol{x}_1, ..., \boldsymbol{x}_m, \boldsymbol{u}).
\end{aligned} \tag{1}$$

The objective function $J$ is the negative total potential energy of the system in the equilibrium state, where $\Pi$ is the total potential energy of the equilibrated system, and $\boldsymbol{u}(\boldsymbol{x}_1, ..., \boldsymbol{x}_m)$ is the equilibrating displacement field (state variable). The term $V_{\max}^j$ is the prescribed upper bound on the total volume associated with the $j$th volume constraint, $g^j$; $x_{\min}$ and $x_{\max}$ are the lower and upper bounds of the design variables; $x_i^{(e)}$ is the cross-sectional area of truss member $e$ with the $i$th material; $\boldsymbol{L}_i$ is the length vector corresponding to the $i$th material; $M_i$ is the number of truss members in the ground structure of the $i$th material. As a demonstration of the notation in the proposed multi-material optimization formulation (1), Fig. 3 and Table 1 summarize the parameters for a case with four materials ($m = 4$, $M_1 = 5, M_2 = 6, M_3 = 9, M_4 = 9$) and three volume constraints ($nc = 3, \mathscr{G}^1 = \{1, 2\}, \mathscr{G}^2 = \{3\}, \mathscr{G}^3 = \{4\}$).

The total potential energy of the entire system $\Pi$ is defined as

$$\Pi(\boldsymbol{x}_1, ..., \boldsymbol{x}_m, \boldsymbol{u}) = \sum_{i=1}^{m} \sum_{e=1}^{M_i} x_i^{(e)} L_i^{(e)} \Psi_i^{(e)}(\boldsymbol{u}) - \boldsymbol{f}^T \boldsymbol{u}, \tag{2}$$

where $L_i^{(e)}$ and $\Psi_i^{(e)}(\boldsymbol{u})$ are the length and strain energy density function of the $e$th member of material $i$, and $\boldsymbol{f}$ is the external force vector. The strain energy density function, $\Psi_i^{(e)}(\boldsymbol{u})$, is assumed to be convex and differentiable for any

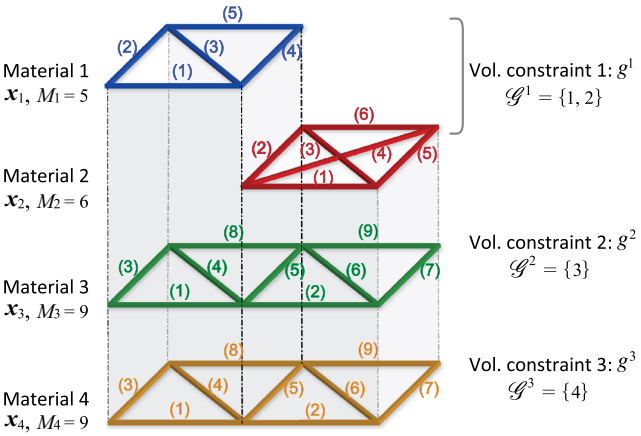


**Fig. 3** Illustration of parameters in multi-material optimization formulation: four materials share & split the design domain ($m = 4$, $M_1 = 5, M_2 = 6, M_3 = 9, M_4 = 9$) with three volume constraints ("Material 1" and "Material 2" share one volume constraint while "Material 3" and "Material 4" have individual constraints, $nc = 3$, $\mathscr{G}^1 = \{1, 2\}, \mathscr{G}^2 = \{3\}, \mathscr{G}^3 = \{4\}$). (Online version in color)

given $\boldsymbol{u}$. The expressions of $\Psi_i^{(e)}(\boldsymbol{u})$ for Ogden and bilinear materials are described in Section 4. According to (2), the total potential energy $\Pi$ is interpolated as a linear function of the design variable (after the strain energy density function of each member, $\Psi_i^{(e)}(\boldsymbol{u})$, is obtained through the nonlinear structural analysis).

Here, we compute the sensitivity for the above optimization formulation. The sensitivity of the objective function is as follows,

$$\begin{aligned}
\frac{\partial J}{\partial x_i^{(e)}}(\boldsymbol{x}_1, ..., \boldsymbol{x}_m) = & -\frac{\partial \Pi}{\partial x_i^{(e)}}(\boldsymbol{x}_1, ..., \boldsymbol{x}_m, \boldsymbol{u}(\boldsymbol{x}_1, ..., \boldsymbol{x}_m)) \\
& - \left[\frac{\partial \Pi}{\partial \boldsymbol{u}}(\boldsymbol{x}_1, ..., \boldsymbol{x}_m, \boldsymbol{u}(\boldsymbol{x}_1, ..., \boldsymbol{x}_m))\right] \\
& \cdot \left[\frac{\partial \boldsymbol{u}}{\partial x_i^{(e)}}(\boldsymbol{x}_1, ..., \boldsymbol{x}_m, \boldsymbol{u}(\boldsymbol{x}_1, ..., \boldsymbol{x}_m))\right].
\end{aligned} \tag{3}$$

Under the assumption of global equilibrium, $\boldsymbol{u}$ is the equilibrating displacement field under external load $\boldsymbol{f}$ in the objective function, therefore, the second term on the right-hand-side of (3) vanishes. By using (2) and the fact that the term $\boldsymbol{f}^T \boldsymbol{u}$ is (explicitly) independent of the design variables, we obtain the sensitivity as

$$\begin{aligned}
\frac{\partial J}{\partial x_i^{(e)}}(\boldsymbol{x}_1, ..., \boldsymbol{x}_m) &= -\frac{\partial \Pi}{\partial x_i^{(e)}}(\boldsymbol{x}_1, ..., \boldsymbol{x}_m, \boldsymbol{u}(\boldsymbol{x}_1, ..., \boldsymbol{x}_m)) \\
&= -L_i^{(e)} \Psi_i^{(e)}(\boldsymbol{u}(\boldsymbol{x}_1, ..., \boldsymbol{x}_m)).
\end{aligned} \tag{4}$$

Note that the sensitivity given by (4) is always non-positive because $L_i^{(e)} \Psi_i^{(e)}(\boldsymbol{u}(\boldsymbol{x}_1, ..., \boldsymbol{x}_m)) \geq 0$, and the computation of sensitivity does not involve an adjoint vector. The

**Table 1** Illustration of parameters in multi-material optimization formulation (Fig. 3)

| | | |
|---|---|---|
| Materials, $m = 4$ | $M_i$ | $\boldsymbol{x}_i = \{x_i^{(e)}\}^T, \quad i = 1, ..., m, \quad e = 1, ..., M_i$ |
| 1 | $M_1 = 5$ | $\boldsymbol{x}_1 = \{x_1^{(1)}, x_1^{(2)}, x_1^{(3)}, x_1^{(4)}, x_1^{(5)}\}^T$ |
| 2 | $M_2 = 6$ | $\boldsymbol{x}_2 = \{x_2^{(1)}, x_2^{(2)}, x_2^{(3)}, x_2^{(4)}, x_2^{(5)}, x_2^{(6)}\}^T$ |
| 3 | $M_3 = 9$ | $\boldsymbol{x}_3 = \{x_3^{(1)}, x_3^{(2)}, x_3^{(3)}, x_3^{(4)}, x_3^{(5)}, x_3^{(6)}, x_3^{(7)}, x_3^{(8)}, x_3^{(9)}\}^T$ |
| 4 | $M_4 = 9$ | $\boldsymbol{x}_4 = \{x_4^{(1)}, x_4^{(2)}, x_4^{(3)}, x_4^{(4)}, x_4^{(5)}, x_4^{(6)}, x_4^{(7)}, x_4^{(8)}, x_4^{(9)}\}^T$ |
| Vol. constraints, $nc = 3$ | $\mathscr{G}^j$ | $g^j = \sum_{i \in \mathscr{G}^j} \boldsymbol{L}_i^{\mathrm{T}} \boldsymbol{x}_i - V_{\max}^j \le 0, \quad j = 1, ..., nc$ |
| 1 | $\mathscr{G}^1 = \{1, 2\}$ | $g^1 = \boldsymbol{L}_1^{\mathrm{T}} \boldsymbol{x}_1 + \boldsymbol{L}_2^{\mathrm{T}} \boldsymbol{x}_2 - V_{\max}^1 \le 0$ |
| 2 | $\mathscr{G}^2 = \{3\}$ | $g^2 = \boldsymbol{L}_3^{\mathrm{T}} \boldsymbol{x}_3 - V_{\max}^2 \le 0$ |
| 3 | $\mathscr{G}^3 = \{4\}$ | $g^3 = \boldsymbol{L}_4^{\mathrm{T}} \boldsymbol{x}_4 - V_{\max}^3 \le 0$ |

sensitivity of the $j$th volume constraint for member $e$ is calculated as

$$\frac{\partial g^j(\boldsymbol{x}_1, ..., \boldsymbol{x}_m)}{\partial x_i^{(e)}} = \begin{cases} L_i^{(e)} & \text{if} \quad i \in \mathscr{G}^j, \\ 0 & \text{otherwise.} \end{cases} \tag{5}$$

### 2.2 KKT conditions

In this subsection, we show the KKT conditions of the multi-material optimization formulation (1). To derive the KKT conditions, the Lagrangian takes the following form by introducing a set of Lagrange multipliers $\overline{\phi}_V^j$, $j = 1, ..., nc$, corresponding to the volume constraints:

$$\overline{\mathscr{L}}\left(\boldsymbol{x}_1, ..., \boldsymbol{x}_m, \overline{\phi}_V^1, ..., \overline{\phi}_V^{nc}\right) = J(\boldsymbol{x}_1, ..., \boldsymbol{x}_m) + \sum_{j=1}^{nc} \overline{\phi}_V^j \left( \sum_{i \in \mathscr{G}^j} \boldsymbol{L}_i^{\mathrm{T}} \boldsymbol{x}_i - V_{\max}^j \right). \tag{6}$$

If we denote $\boldsymbol{x}_1^*, ..., \boldsymbol{x}_m^*$ as the optimal solutions of design variables and $\overline{\phi}_V^{1,*}, ..., \overline{\phi}_V^{nc,*}$ as the corresponding Lagrange multipliers; for any $i \in \mathscr{G}^j$, $j = 1, ..., nc$, we have:

$$\frac{\partial \overline{\mathscr{L}}}{\partial x_i^{(e)}}\left(\boldsymbol{x}_1^*, ..., \boldsymbol{x}_m^*, \overline{\phi}_V^{1,*}, ..., \overline{\phi}_V^{nc,*}\right) \le 0, \quad \text{if} \quad x_i^{(e),*} = x_{\max}, \tag{7}$$

$$\frac{\partial \overline{\mathscr{L}}}{\partial x_i^{(e)}}\left(\boldsymbol{x}_1^*, ..., \boldsymbol{x}_m^*, \overline{\phi}_V^{1,*}, ..., \overline{\phi}_V^{nc,*}\right) = 0, \quad \text{if} \quad x_{\min} < x_i^{(e),*} < x_{\max}, \tag{8}$$

$$\frac{\partial \overline{\mathscr{L}}}{\partial x_i^{(e)}}\left(\boldsymbol{x}_1^*, ..., \boldsymbol{x}_m^*, \overline{\phi}_V^{1,*}, ..., \overline{\phi}_V^{nc,*}\right) \ge 0, \quad \text{if} \quad x_i^{(e),*} = x_{\min}, \tag{9}$$

where the derivative of the Lagrangian is given by

$$\frac{\partial \overline{\mathscr{L}}}{\partial x_i^{(e)}}\left(\boldsymbol{x}_1, ..., \boldsymbol{x}_m, \overline{\phi}_V^1, ..., \overline{\phi}_V^{nc}\right) = -L_i^{(e)} \Psi_i^{(e)}\left(\boldsymbol{u}\left(\boldsymbol{x}_1, ..., \boldsymbol{x}_m\right)\right) + \overline{\phi}_V^j L_i^{(e)}, \quad \forall i \in \mathscr{G}^j. \tag{10}$$

Combining (10) with (7)–(9), we obtain the KKT conditions for the optimal solution $\left(\boldsymbol{x}_1^*, ..., \boldsymbol{x}_m^*, \overline{\phi}_V^{1,*}, ..., \overline{\phi}_V^{nc,*}\right)$ of the optimization formulation (1) as follows (for any $i \in \mathscr{G}^j$, $j = 1, ..., nc$):

$$\Psi_i^{(e)}\left(\boldsymbol{u}\left(\boldsymbol{x}_1^*, ..., \boldsymbol{x}_m^*\right)\right) \ge \overline{\phi}_V^{j,*}, \quad \text{if} \quad x_i^{(e),*} = x_{\max}, \tag{11}$$

$$\Psi_i^{(e)}\left(\boldsymbol{u}\left(\boldsymbol{x}_1^*, ..., \boldsymbol{x}_m^*\right)\right) = \overline{\phi}_V^{j,*}, \quad \text{if} \quad x_{\min} < x_i^{(e),*} < x_{\max}, \tag{12}$$

$$\Psi_i^{(e)}\left(\boldsymbol{u}\left(\boldsymbol{x}_1^*, ..., \boldsymbol{x}_m^*\right)\right) \le \overline{\phi}_V^{j,*}, \quad \text{if} \quad x_i^{(e),*} = x_{\min}. \tag{13}$$

From (12), we observe that at the optimal design, the strain energy density values for the members (with inactive box constraints) within the same volume constraint are identical (equal to the optimal solution of the associated Lagrange multiplier, $\overline{\phi}_V^{j,*}$), regardless of the material type. This idea is further verified by a numerical example in Section 5.3. For instance, let's assume that "Material 1" and "Material 2" have different material models. If these two materials are assigned to one constraint, the members associated with "Material 1" and "Material 2" in the optimal design should have the same values of strain energy density (even though the material behaviors differ). This observation concerning multi-material topology optimization is analogous to the full-stress design in the linear case with single material (Christensen and Klarbring 2009).

### 2.3 Incorporation of the discrete filter into the proposed multi-material formulation

To improve the computational efficiency and define structures that satisfy global equilibrium, we implement the discrete filter (Ramos and Paulino 2016; Zhang et al. 2017) into the nonlinear multi-material topology optimization framework in (1). Denoting $\alpha_f$ as the filter parameter for controlling the resolution of the topology, we introduce the filter operation as follows:

$$Filter\left(\boldsymbol{x}, \alpha_f, e\right) = \begin{cases} 0 & \text{if } \frac{x^{(e)}}{max(\boldsymbol{x})} < \alpha_f < 1, \\ x^{(e)} & \text{otherwise.} \end{cases} \tag{14}$$

We perform the filter operation during the optimization process to remove the information associated with the set of truss members with normalized areas below the filter parameter $\alpha_f$. Therefore the complete multi-material topology optimization formulation with the discrete filter is as follows:

$$
\begin{aligned}
\min_{\boldsymbol{x}_1,\ldots,\boldsymbol{x}_m} \quad & J\left(\boldsymbol{x}_1,\ldots,\boldsymbol{x}_m\right) = \min_{\boldsymbol{x}_1,\ldots,\boldsymbol{x}_m} \; -\Pi\left(\overline{\boldsymbol{x}}_1(\boldsymbol{x}_1),\ldots,\overline{\boldsymbol{x}}_m(\boldsymbol{x}_m),\boldsymbol{u}\left(\boldsymbol{x}_1,\ldots,\boldsymbol{x}_m\right)\right) \\
\text{s.t.} \quad & g^j\left(\boldsymbol{x}_1,\ldots,\boldsymbol{x}_m\right) = \sum_{i\in\mathscr{G}^j} \boldsymbol{L}_i^{\mathrm{T}}\overline{\boldsymbol{x}}_i(\boldsymbol{x}_i) - V_{\max}^j \le 0, \;\; j = 1,\ldots,nc, \\
& 0 \le x_i^{(e)} \le x_{\max}, \; i = 1,\ldots,m, \;\text{and}\; e = 1,\ldots,M_i, \\
\text{with } & \boldsymbol{u}\left(\boldsymbol{x}_1,\ldots,\boldsymbol{x}_m\right) = \arg\min_{\boldsymbol{u}} \left\{\Pi\left(\overline{\boldsymbol{x}}_1(\boldsymbol{x}_1),\ldots,\overline{\boldsymbol{x}}_m(\boldsymbol{x}_m),\boldsymbol{u}\right) + \frac{\Gamma}{2}\boldsymbol{u}^{\mathrm{T}}\boldsymbol{u}\right\}, \\
& \overline{x}_i^{(e)} = Filter\left(\boldsymbol{x}_i,\alpha_f,e\right), \;\; i = 1,\ldots,m, \;\text{and}\; e = 1,\ldots,M_i,
\end{aligned}
\tag{15}
$$

where $\overline{\boldsymbol{x}}_i$ denotes the filtered design variables associated with the $i$th material. In formulation (15), the lower bound is taken as $x_{\min} = 0$ to account for the removal of members, which transforms the sizing problem in (1) into a topology optimization problem. A Tikhonov regularization term $\frac{\Gamma}{2}\boldsymbol{u}^{\mathrm{T}}\boldsymbol{u}$ is added to the total potential energy in the state equation to prevent singular stiffness matrices (Tikhonov and Arsenin 1977; Felippa n.d; Ramos and Paulino 2016; Talischi and Paulino 2013).

### 2.4 Remarks

The properties of the proposed multi-material topology optimization framework relate to several aspects. *First,* the optimization formulations in (1) and (15) are capable of handling a general number of materials. The constitutive relationship of each material is flexible (e.g., linear, bilinear, or nonlinear). For example, we can obtain a variety of materials by changing the parameters of the Ogden-based model (see Section 4). *Second,* the choice of the specific material model is independent for each material. For instance, we can use an Ogden-based model for certain material layers and a bilinear model for others. *Third,* in the optimization formulation, the assignment of volume constraints for multiple materials contains general scenarios, meaning that the number of volume constraints satisfies the relation $1 \le nc \le m$. As a demonstration, Table 2 summarizes three possible combinations of volume constraints if three materials ($m = 3$) are used in the optimization problem. Figure 4 shows the three representative scenarios of the volume constraint assignment, i.e., sharing (Fig. 4c), splitting (Fig. 4d), and a combination of sharing & splitting (Fig. 4e). The case of assigning a total/global volume constraint to all materials corresponds to $nc = 1$ and $\mathscr{G}^1 = \{1, 2, 3\}$ (Fig. 4c), and the case of assigning individual volume constraint to each material corresponds to $nc = m = 3$, $\mathscr{G}^1 = \{1\}, \mathscr{G}^2 = \{2\}, \mathscr{G}^3 = \{3\}$ (Fig. 4d). To handle an arbitrary number of volume constraints, we propose a unified design update scheme in Section 3. This update scheme performs efficient and robust updates of the design variables associated with each volume constraint in an independent fashion.

**Table 2** Three possible combinations of volume constraints for three materials

| Materials | Scenarios of volume constraints | | |
|---|---|---|---|
| | (Fig. 4c) | (Fig. 4d) | (Fig. 4e) |
| 1 | $V_{\max}^1$ | $V_{\max}^1$ | $V_{\max}^1$ |
| 2 | | $V_{\max}^2$ | $V_{\max}^2$ |
| 3 | | $V_{\max}^3$ | |

## 3 The ZPR design update scheme

In this section, we present the ZPR (zipper, phonetically) design update scheme. In the proposed multi-material formulations in (1) and (15), we have multiple ($nc$) volume constraints. Accordingly, we need an update scheme that can handle multiple constraints. The standard OC method is a robust and efficient update scheme for single material topology optimization, however, it only handles a single volume constraint. Consequently, the OC method cannot be directly applied to the proposed multi-material formulations in (1) and (15), unless only one volume constraint is used, i.e., $nc = 1$. To address such limitation, we present the ZPR design update scheme, which is capable of handling an arbitrary number of volume constraints while preserving the efficiency and effectiveness of the standard OC method. The proposed ZPR design update scheme allows for the separation and independent updating of design variables associated with each volume constraint. In computational implementations, the ZPR update scheme loops over the set of volume constraints. For the $j$th volume constraint,

only the associated design variables are updated by using the Lagrange multiplier associated with the $j$th volume constraint.

In the remainder of this section, we present the derivation of the ZPR design update scheme for the proposed optimization formulation in (1) containing an arbitrary number of volume constraints ($nc$). The first step of the derivation is to perform an explicit convex approximation of the objective at each optimization step (Christensen and Klarbring 2009). In this convex approximation, we first introduce a set of intervening variables $\boldsymbol{y}_i(\boldsymbol{x}_i)$ such that $y_i^{(e)}(x_i^{(e)}) = (x_i^{(e)})^{-\alpha}$, $i = 1, ..., m$, and $e = 1, ..., M_i$, where $\alpha$ is an arbitrary and strictly positive number. At the $k$th optimization step, we then approximate the objective function as a linear function of $\boldsymbol{y}_i$ as follows:

$$\begin{aligned} J(\boldsymbol{x}_1, ..., \boldsymbol{x}_m) \approx J^k(\boldsymbol{x}_1, ..., \boldsymbol{x}_m) &= J\left(\boldsymbol{x}_1^k, ..., \boldsymbol{x}_m^k\right) \\ &+ \sum_{i=1}^{m} \left[\frac{\partial J}{\partial \boldsymbol{y}_i}\left(\boldsymbol{x}_1^k, ..., \boldsymbol{x}_m^k\right)\right]^T \left[\boldsymbol{y}_i(\boldsymbol{x}_i) - \boldsymbol{y}_i\left(\boldsymbol{x}_i^k\right)\right] \\ &= J\left(\boldsymbol{x}_1^k, ..., \boldsymbol{x}_m^k\right) \\ &+ \sum_{i=1}^{m} \left[\boldsymbol{b}_i\left(\boldsymbol{x}_1^k, ..., \boldsymbol{x}_m^k\right)\right]^T \left[\boldsymbol{y}_i(\boldsymbol{x}_i) - \boldsymbol{y}_i\left(\boldsymbol{x}_i^k\right)\right], \quad (16) \end{aligned}$$

where $\boldsymbol{x}_i^k$ and $\boldsymbol{y}_i(\boldsymbol{x}_i^k)$ are the design and intervening variables, respectively, at the $k$th optimization step of material $i$. Notice that for a given optimization step $k$, the vector $\boldsymbol{b}_i\left(\boldsymbol{x}_1^k, ..., \boldsymbol{x}_m^k\right)$ is a constant vector whose component $(e)$ is given by

$$\begin{aligned} b_i^{(e)}\left(\boldsymbol{x}_1^k, ..., \boldsymbol{x}_m^k\right) &= \frac{\partial J}{\partial y_i^{(e)}}\left(\boldsymbol{x}_1^k, ..., \boldsymbol{x}_m^k\right) \\ &= -\frac{\left(x_i^{(e),k}\right)^{1+\alpha}}{\alpha} \frac{\partial J}{\partial x_i^{(e)}}\left(\boldsymbol{x}_1^k, ..., \boldsymbol{x}_m^k\right), \quad (17) \end{aligned}$$

where $\partial J / \partial x_i^{(e)}(\boldsymbol{x}_1^k, ..., \boldsymbol{x}_m^k)$ is the $e$th component of the sensitivity vector of the $i$th material at step $k$. Therefore, the approximated subproblem of the original problem at the $k$th step is given by

$$\begin{aligned} \min_{\boldsymbol{x}_1,...,\boldsymbol{x}_m} \; & J^k(\boldsymbol{x}_1, ..., \boldsymbol{x}_m) = \min_{\boldsymbol{x}_1,...,\boldsymbol{x}_m} \sum_{i=1}^{m} \left[\boldsymbol{b}_i(\boldsymbol{x}_1^k, ..., \boldsymbol{x}_m^k)\right]^T \boldsymbol{y}_i(\boldsymbol{x}_i) \\ \text{s.t.} \; & \sum_{i \in \mathscr{G}^j} \boldsymbol{L}_i^{\mathrm{T}} \boldsymbol{x}_i - V_{\max}^j \le 0, \quad j = 1, ..., nc, \quad (18) \\ & x_{i,\mathrm{L}}^{(e),k} \le x_i^{(e)} \le x_{i,\mathrm{U}}^{(e),k}, \; i = 1, ..., m, \text{ and } e = 1, ..., M_i, \\ & \text{with } y_i^{(e)}(x_i^{(e)}) = (x_i^{(e)})^{-\alpha}, \; i = 1, ..., m, \text{ and } e = 1, ..., M_i, \end{aligned}$$

where $x_{i,\mathrm{L}}^{(e),k} = \max(x_{\min}, x_i^{(e),k} - move)$ and $x_{i,\mathrm{U}}^{(e),k} = \min(x_{\max}, x_i^{(e),k} + move)$ are the lower and upper bounds of the design variables in the subproblem, and $move$ is the prescribed move limit. In vector notation, the lower and upper

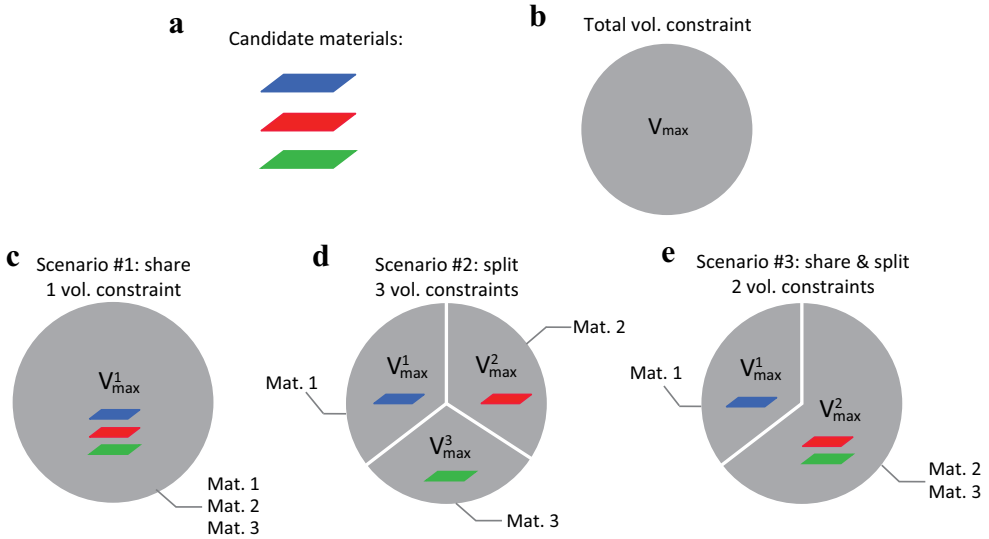


**Fig. 4** Potential combination of volume constraints: **a** Candidate materials; **b** total volume constraint, $V_{\max}$; **c** Scenario #1: three materials share the (single) total volume constraint, $nc = 1$, $\mathscr{G}^1 = \{1, 2, 3\}$; **d** Scenario #2: three materials split the total volume constraint, (i.e., each material is associated with an individual constraint, $nc = 3$, $\mathscr{G}^1 = \{1\}, \mathscr{G}^2 = \{2\}, \mathscr{G}^3 = \{3\}$); **e** Scenario #3: three materials share & split the volume constraint (i.e., "Material 1" has an individual constraint while both "Material 2" and "Material 3" share another volume constraint, $nc = 2$, $\mathscr{G}^1 = \{1\}$, $\mathscr{G}^2 = \{2, 3\}$). (Online version in color)

bounds are denoted as $\boldsymbol{x}_{i,\mathrm{L}}^k$ and $\boldsymbol{x}_{i,\mathrm{U}}^k$. When we introduce a set of Lagrange multipliers $\phi_V^j$ for each volume constraint, the above Lagrangian function of the subproblem in (18) takes the form

$$\begin{aligned}\mathscr{L}^k\left(\boldsymbol{x}_1,...,\boldsymbol{x}_m,\phi_V^1,...,\phi_V^{nc}\right) &= \sum_{i=1}^{m}\left[\boldsymbol{b}_i\left(\boldsymbol{x}_1^k,...,\boldsymbol{x}_m^k\right)\right]^T\boldsymbol{y}_i(\boldsymbol{x}_i)+\sum_{j=1}^{nc}\phi_V^j\left(\sum_{i\in\mathscr{G}^j}\boldsymbol{L}_i^{\mathrm{T}}\boldsymbol{x}_i-V_{\max}^j\right)\\ &= \sum_{j=1}^{nc}\left\{\sum_{i\in\mathscr{G}^j}\left[\left[\boldsymbol{b}_i\left(\boldsymbol{x}_1^k,...,\boldsymbol{x}_m^k\right)\right]^T\boldsymbol{y}_i(\boldsymbol{x}_i)+\phi_V^j\boldsymbol{L}_i^{\mathrm{T}}\boldsymbol{x}_i\right]-\phi_V^jV_{\max}^j\right\}. \end{aligned}\tag{19}$$

The dual objective function is given by

$$\begin{aligned}\mathscr{D}^k\left(\phi_V^1,...,\phi_V^{nc}\right) &= \min_{\boldsymbol{x}_{1,\mathrm{L}}^k\le\boldsymbol{x}_1\le\boldsymbol{x}_{1,\mathrm{U}}^k,...,\boldsymbol{x}_{m,\mathrm{L}}^k\le\boldsymbol{x}_m\le\boldsymbol{x}_{m,\mathrm{U}}^k}\mathscr{L}^k\left(\boldsymbol{x}_1,...,\boldsymbol{x}_m,\phi_V^1,...,\phi_V^{nc}\right)\\ &= \sum_{j=1}^{nc}\left\{\min_{\boldsymbol{x}_{i,\mathrm{L}}^k\le\boldsymbol{x}_{i\in\mathscr{G}^j}\le\boldsymbol{x}_{i,\mathrm{U}}^k}\sum_{i\in\mathscr{G}^j}\left[\left[\boldsymbol{b}_i\left(\boldsymbol{x}_1^k,...,\boldsymbol{x}_m^k\right)\right]^T\boldsymbol{y}_i(\boldsymbol{x}_i)+\phi_V^j\boldsymbol{L}_i^{\mathrm{T}}\boldsymbol{x}_i\right]-\phi_V^jV_{\max}^j\right\}. \end{aligned}\tag{20}$$

Notice that the dual objective function has a clear separable structure and thus can be recast as $\mathscr{D}^k\left(\phi_V^1,...,\phi_V^{nc}\right)=\sum_{j=1}^{nc}\mathscr{D}^{j,k}\left(\phi_V^j\right)$, where $\mathscr{D}^{j,k}\left(\phi_V^j\right)$ has the form

$$\mathscr{D}^{j,k}\left(\phi_V^j\right)=\min_{\boldsymbol{x}_{i,\mathrm{L}}^k\le\boldsymbol{x}_{i\in\mathscr{G}^j}\le\boldsymbol{x}_{i,\mathrm{U}}^k}\sum_{i\in\mathscr{G}^j}\left\{\left[\boldsymbol{b}_i\left(\boldsymbol{x}_1^k,...,\boldsymbol{x}_m^k\right)\right]^T\boldsymbol{y}_i(\boldsymbol{x}_i)+\phi_V^j\boldsymbol{L}_i^{\mathrm{T}}\boldsymbol{x}_i\right\}-\phi_V^jV_{\max}^j.\tag{21}$$

The optimality condition of the first term on the right-hand-side of (21) takes the form

$$\begin{aligned}\frac{\partial\left\{\left[\boldsymbol{b}_i\left(\boldsymbol{x}_1^k,...,\boldsymbol{x}_m^k\right)\right]^T\boldsymbol{y}_i(\boldsymbol{x}_i)+\phi_V^j\boldsymbol{L}_i^{\mathrm{T}}\boldsymbol{x}_i\right\}}{\partial x_i^{(e)}} &= -\alpha b_i^{(e)}\left(\boldsymbol{x}_1^k,...,\boldsymbol{x}_m^k\right)\\ &\quad\times\left(x_i^{(e)}\right)^{(-\alpha-1)}\\ &\quad+\phi_V^jL_i^{(e)}=0,\quad\forall i\in\mathscr{G}^j,\end{aligned}\tag{22}$$

which gives

$$x_i^{(e)*}=Q_i^{(e),k}\left(\phi_V^j\right)=\left[\frac{\alpha b_i^{(e)}\left(\boldsymbol{x}_1^k,...,\boldsymbol{x}_m^k\right)}{\phi_V^j\,L_i^{(e)}}\right]^{\frac{1}{1+\alpha}},\quad\forall i\in\mathscr{G}^j.\tag{23}$$

Having obtained $x_i^{(e)*}$, we then check if the assumption that it is within the interval $\left[x_{i,L}^{(e),k},x_{i,U}^{(e),k}\right]$ holds. The final form of the primal-dual relationship is given by

$$x_i^{(e)*}=Q_i^{(e),k}\left(\phi_V^j\right)=\begin{cases}x_{i,\mathrm{L}}^{(e),k} & \text{if }\left[\frac{\alpha b_i^{(e)}\left(\boldsymbol{x}_1^k,...,\boldsymbol{x}_m^k\right)}{\phi_V^j\,L_i^{(e)}}\right]^{\frac{1}{1+\alpha}}<x_{i,\mathrm{L}}^{(e),k}\\ \left[\frac{\alpha b_i^{(e)}\left(\boldsymbol{x}_1^k,...,\boldsymbol{x}_m^k\right)}{\phi_V^j\,L_i^{(e)}}\right]^{\frac{1}{1+\alpha}} & \text{if }x_{i,\mathrm{L}}^{(e),k}\le\left[\frac{\alpha b_i^{(e)}\left(\boldsymbol{x}_1^k,...,\boldsymbol{x}_m^k\right)}{\phi_V^j\,L_i^{(e)}}\right]^{\frac{1}{1+\alpha}}\le x_{i,\mathrm{U}}^{(e),k}\\ x_{i,\mathrm{U}}^{(e),k} & \text{if }\left[\frac{\alpha b_i^{(e)}\left(\boldsymbol{x}_1^k,...,\boldsymbol{x}_m^k\right)}{\phi_V^j\,L_i^{(e)}}\right]^{\frac{1}{1+\alpha}}>x_{i,\mathrm{U}}^{(e),k}\end{cases},\quad\forall i\in\mathscr{G}^j.\tag{24}$$

Inserting the above primal-dual relation into the dual function, we obtain the dual problem:

$$\max_{\phi_V^1,\ldots,\phi_V^{nc}} \mathscr{D}^k\left(\phi_V^1,\ldots,\phi_V^{nc}\right) = \sum_{j=1}^{nc} \max_{\phi_V^j} \mathscr{D}^{j,k}\left(\phi_V^j\right). \tag{25}$$

Notice that the dual objective function is also separable, and the stationary condition with respect to $\phi_V^j$ yields:

$$\frac{\partial \mathscr{D}^k}{\partial \phi_V^j} = \sum_{i\in\mathscr{G}^j} \sum_{e=1}^{M_i} L_i^{(e)}\, x_i^{(e)*}\left(\phi_V^j\right) - V_{\max}^j = 0. \tag{26}$$

Observe that the above equation is a monotonic algebraic equation of $\phi_V^j$ (Christensen and Klarbring 2009), and thus can be solved by various algorithms, such as the bisection method. In addition, the calculation of the Lagrange multipliers can be done independently. We hereby denote $\phi_V^{j*}$ as the solution to the $j$th of (26). The update of the $e$th component of the design variables then takes the form:

$$x_i^{(e),k+1} = Q_i^{(e),k}\left(\phi_V^{j*}\right), \quad \forall i \in \mathscr{G}^j. \tag{27}$$

By plugging in the sensitivity information (4), a simplified expression for the design variable update of the ZPR update scheme can be obtained as

$$x_i^{(e),k+1} = \begin{cases} x_{i,\mathrm{L}}^{(e),k} & \text{if } \left[\dfrac{\Psi_i^{(e)}\left(\boldsymbol{u}\left(\boldsymbol{x}_1^k,\ldots,\boldsymbol{x}_m^k\right)\right)}{\phi_V^{j*}}\right]^\eta x_i^{(e),k} < x_{i,\mathrm{L}}^{(e),k} \\ \left[\dfrac{\Psi_i^{(e)}\left(\boldsymbol{u}\left(\boldsymbol{x}_1^k,\ldots,\boldsymbol{x}_m^k\right)\right)}{\phi_V^{j*}}\right]^\eta x_i^{(e),k} & \text{if } x_{i,\mathrm{L}}^{(e),k} \le \left[\dfrac{\Psi_i^{(e)}\left(\boldsymbol{u}\left(\boldsymbol{x}_1^k,\ldots,\boldsymbol{x}_m^k\right)\right)}{\phi_V^{j*}}\right]^\eta x_i^{(e),k} \le x_{i,\mathrm{U}}^{(e),k} \\ x_{i,\mathrm{U}}^{(e),k} & \text{if } \left[\dfrac{\Psi_i^{(e)}\left(\boldsymbol{u}\left(\boldsymbol{x}_1^k,\ldots,\boldsymbol{x}_m^k\right)\right)}{\phi_V^{j*}}\right]^\eta x_i^{(e),k} > x_{i,\mathrm{U}}^{(e),k} \end{cases}, \quad \forall i \in \mathscr{G}^j. \tag{28}$$

In the above expression, the parameter $\eta$ is introduced as $\eta = 1/(1+\alpha)$, which is commonly referred as the damping factor. It can be either constant (e.g. Christensen and Klarbring 2009) or adaptive (Groenwold and Etman 2008).

We remark that from (27) and (28), the update of the design variable depends only on the Lagrange multiplier of the corresponding volume constraint. Therefore, in the case of multiple volume constraints, the design variables associated with each volume constraint can be updated independently. Note that because the update of design variables in each volume constraint is independent, the update can be done either in sequence or in parallel. The procedure of multi-material topology optimization with the ZPR design update scheme using sequential updates is illustrated in Algorithm 1.

**Algorithm 1** Multi-material topology optimization with the ZPR design update scheme

**Initialize:** $\boldsymbol{x}_1^0, \ldots, \boldsymbol{x}_m^0$, $\mathrm{iter}_{\max}$, $\mathrm{tol}_{\mathrm{opt}}$
**for** $k = 0, 1, \ldots, \mathrm{iter}_{\max}$ **do**
  Solve: $\boldsymbol{u}\left(\boldsymbol{x}_1^k, \ldots, \boldsymbol{x}_m^k\right) = \arg\min_{\boldsymbol{u}} \left[\Pi\left(\boldsymbol{x}_1^k, \ldots, \boldsymbol{x}_m^k, \boldsymbol{u}\right)\right]$
  Compute: $J\left(\boldsymbol{x}_1^k, \ldots, \boldsymbol{x}_m^k\right)$, $g^j\left(\boldsymbol{x}_1^k, \ldots, \boldsymbol{x}_m^k\right)$, $\partial J\left(\boldsymbol{x}_1^k, \ldots, \boldsymbol{x}_m^k\right)/\partial x_i^{(e)}$, and $\partial g^j\left(\boldsymbol{x}_1^k, \ldots, \boldsymbol{x}_m^k\right)/\partial x_i^{(e)}$
  **for** $j = 1, 2, \ldots, nc$ **do**
    Compute $\phi_{V*}^j$ by solving (26)
    Update $x_i^{(e),k+1} = Q_i^{(e),k}\left(\phi_V^{j*}\right)$, $\forall i \in \mathscr{G}^j$ according to (28)
  **end for**
  **if** $\max\left(||\boldsymbol{x}_1^{k+1} - \boldsymbol{x}_1^k||_\infty, \ldots, ||\boldsymbol{x}_m^{k+1} - \boldsymbol{x}_m^k||_\infty\right) < \mathrm{tol}_{\mathrm{opt}}$ **then**
    quit
  **end if**
**end for**
Remove aligned nodes
Plot final topology

## 4 Material nonlinear models

In this section, we briefly review the theory of hyperelastic constitutive models on which the structural analysis part of the paper is based. For details of the derivation, readers are referred to the studies by Ramos and Paulino (2015) and Zhang et al. (2017). For the kinematics and constitutive models, we assume small deformation kinematics and nonlinear constitutive relationships. We compute the linearized stretch $\lambda$ for the truss element as (see, for example, Bonet and Wood 2008):

$$\lambda = 1 + \frac{\boldsymbol{N}^{\mathrm{T}}\left(\boldsymbol{u}_q - \boldsymbol{u}_p\right)}{L}, \tag{29}$$

where $\boldsymbol{N}$ is the unit directional vector of the truss member, $\boldsymbol{u}_p$ and $\boldsymbol{u}_q$ are the nodal displacement vectors of nodes $p$ and $q$ of the element, and $L$ is the length of the element. We account for nonlinear constitutive relationships by using the energy density function based on Ogden (1984), which allows various materials to be represented and has the capability to reproduce a variety of hyperelastic models. The

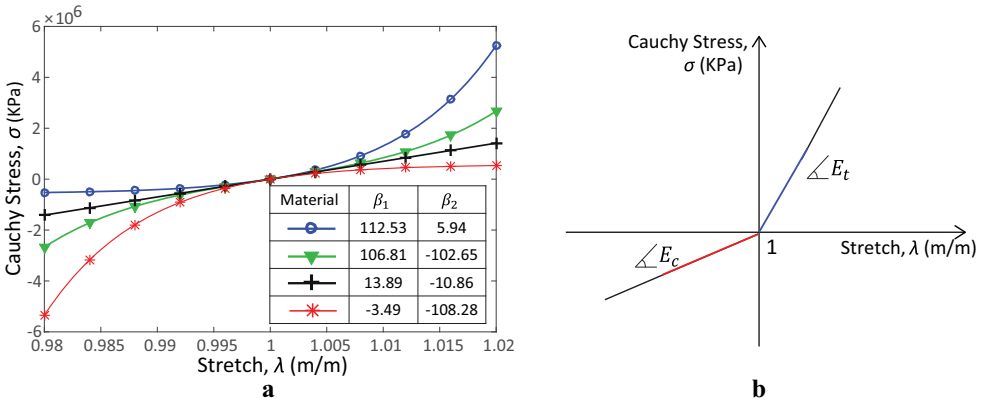


**Fig. 5** Material models: **a** Hyperelastic Ogden-based models with different parameters $(\beta_1, \beta_2)$; **b** bilinear material model with elastic behavior (different Young's moduli for tension and for compression)

strain energy density function for this hyperelastic Ogden material is as follows:

$$\Psi_{OG}\left(\lambda_1, \lambda_2, \lambda_3\right) = \sum_{j=1}^{M} \frac{\gamma_j}{\beta_j}\left(\lambda_1^{\beta_j} + \lambda_2^{\beta_j} + \lambda_3^{\beta_j} - 3\right), \quad (30)$$

where $\lambda_1, \lambda_2, \lambda_3$ denote the principal stretches in three directions, and $M$, $\gamma_j$, and $\beta_j$ are material parameters. For truss members, if we assume that $\lambda_1$ is the axial stretch, namely, $\lambda_1 = \lambda$, and the stretches in the other two directions are taken to be $\lambda_2 = \lambda_3 = 1$. Then (30) can be rewritten as

$$\hat{\Psi}_{OG}\left(\lambda\right) = \sum_{j=1}^{M} \frac{\gamma_j}{\beta_j}\left(\lambda^{\beta_j} - 1\right). \quad (31)$$

Therefore, for the Ogden-based model with $M = 2$ and $\gamma_2 = -\gamma_1$, the principal (Cauchy) stress is obtained as

$$\sigma_{OG}\left(\lambda\right) = \frac{\mathrm{d}\hat{\Psi}_{OG}}{\mathrm{d}\lambda}\left(\lambda\right) = \gamma_1\left(\lambda^{\beta_1 - 1} - \lambda^{\beta_2 - 1}\right). \quad (32)$$

The tangent modulus is then obtained as follows:

$$E_T\left(\lambda\right) = \frac{\mathrm{d}\sigma_{OG}}{\mathrm{d}\lambda}\left(\lambda\right) = \gamma_1\left[\left(\beta_1 - 1\right)\lambda^{\beta_1 - 2} - \left(\beta_2 - 1\right)\lambda^{\beta_2 - 2}\right]. \quad (33)$$

The tangent modulus (in an undeformed state) reduces to Young's modulus in linear elasticity, namely,

$$E_T\left(1\right) = \gamma_1\left(\beta_1 - \beta_2\right) = E_0 = \Lambda + 2\mu, \quad (34)$$

where $\Lambda$ and $\mu$ are the Lamé constants. Note that if the parameters satisfy the following conditions: $\beta_1 \geq 1$, $\beta_2 \leq 1$, $\beta_1 \neq \beta_2$, $\gamma_1 > 0$, and subsequently $E_T > 0$ $\left(\mathrm{d}\sigma_{OG}\left(\lambda\right)/\mathrm{d}\lambda > 0\right)$, then the material model is convex, i.e., $\hat{\Psi}_{OG}\left(\lambda\right)$ is convex for $\lambda > 0$. The stress-stretch relationship of the Ogden model is then expressed as

$$\sigma_{OG}\left(\lambda\right) = \frac{E_0}{\beta_1 - \beta_2}\left(\lambda^{\beta_1 - 1} - \lambda^{\beta_2 - 1}\right). \quad (35)$$

By varying the set of parameters $(\beta_1, \beta_2)$, as shown in Fig. 5a, this Ogden-based model generates a variety of material behaviors.

Another constitutive model used in this paper is the bilinear material. The bilinear constitutive model has a kink at the origin (see Fig. 5b). To treat this class of nonsmooth problems, we refer the reader to Klarbring and Rönnqvist (1995). Using the same format of the Ogden-based model to describe the bilinear model, the energy density function is as follows:

$$\Psi_{Bi}\left(\lambda\right) = \begin{cases} \frac{1}{2}E_t\left(\lambda - 1\right)^2 & \text{if } \lambda > 1, \\ \frac{1}{2}E_c\left(\lambda - 1\right)^2 & \text{otherwise,} \end{cases} \quad (36)$$

**Table 3** Brief description of the numerical examples

| Example | Dimension | Material model | Description | Feature |
|---|---|---|---|---|
| 1 | 2D | Two bilinear models | Opposite loads in a simply supported rectangular domain | Verification |
| 2 | 2D | Four Ogden-based models | Opposite loads in a simply supported rectangular domain | Influence of initial material distributions |
| 3 | 2D | Two bilinear and one linear models | Long-span bridge design | Generality of the formulation including combinations of volume constraints |
| 4 | 3D | Two Ogden-based and one linear models | Crane design subjected to multiple load cases | Potentially translational design: from academia to structural engineering practice |

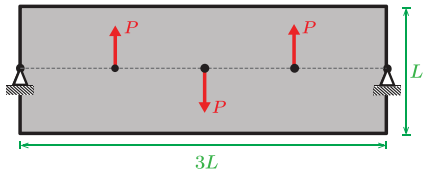


**Fig. 6** Example 1: geometry ($L = 10m$), load ($P = 100kN$), and boundary conditions. The domain is discretized using a $30 \times 10$ grid

where $E_t$ and $E_c$ are Young's moduli for tension and compression, respectively. The stress-stretch relationship for the bilinear material is then obtained as

$$\sigma_{Bi}(\lambda) = \begin{cases} E_t(\lambda - 1) & \text{if } \lambda > 1, \\ E_c(\lambda - 1) & \text{otherwise.} \end{cases} \tag{37}$$

Note that this bilinear material model is always convex as $\mathrm{d}\sigma_{\mathrm{Bi}}(\lambda)/\mathrm{d}\lambda \geq 0$. The term $\mathrm{d}\sigma_{\mathrm{Bi}}(\lambda)/\mathrm{d}\lambda$ may become zero, i.e., $E_t = 0$ or $E_c = 0$.

## 5 Numerical examples

In this section, we provide several numerical examples to demonstrate the proposed multi-material topology optimization using the GSM. Example 1 verifies the proposed multi-material methodology by comparing the results obtained from the proposed scheme with the results obtained from the single material topology optimization.

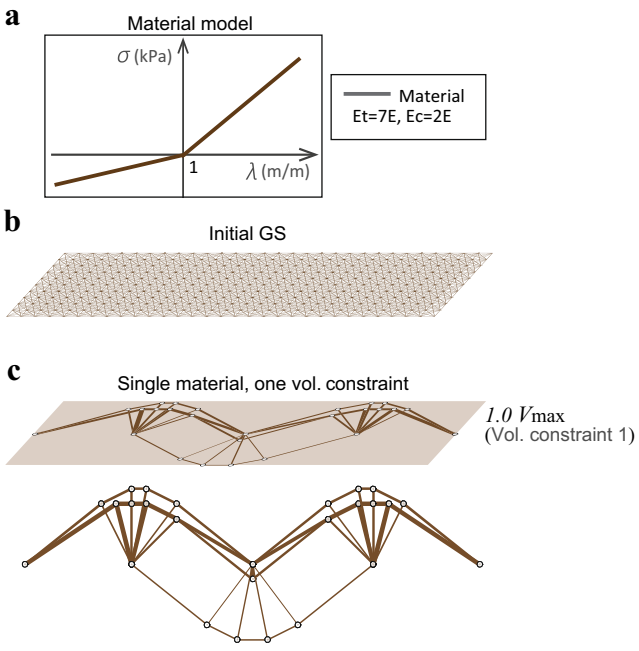


**Fig. 7** Example 1: single material topology optimization. **a** The material model of one bilinear material; **b** the initial level-10 (schematic) GS; **c** the corresponding optimized structure (cf. Fig. 8c). (Online version in color)

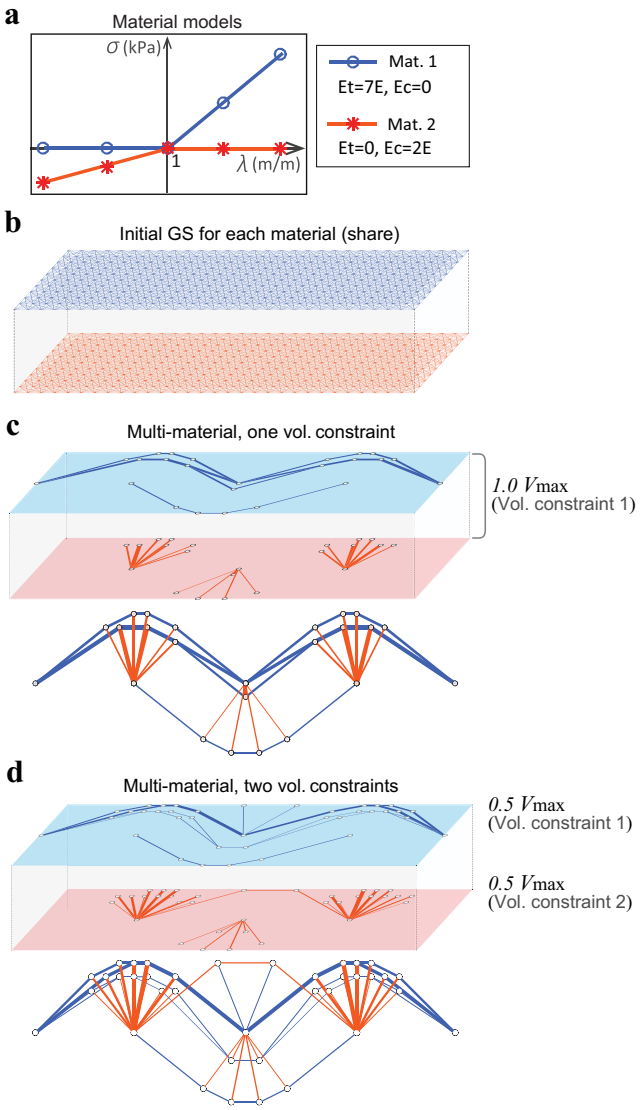


**Fig. 8** Example 1: multi-material topology optimization. **a** Material models of two bilinear materials; **b** two layers of identical initial level-10 (schematic) GSs; **c** the optimized structure of two bilinear materials with one total volume constraint (cf. Fig. 7c); **d** the optimized structure of two bilinear materials with two individual volume constraints. (Online version in color)

Example 2 compares different combination of initial material distributions and their optimized results. Example 3 demonstrates combination of volume constraints and their optimized results. The last example considers multiple load cases and illustrates the application of the proposed multi-material formulation to a 3D crane design using a combination of various material models and general volume constraint setting.

We generate the initial ground structures without overlapped members in each material layer using the collision zone technique by Zegard and Paulino (2014) and Zegard and Paulino (2015) and plot final topologies in 3D using

**Table 4** Numerical information for Example 1 (Figs. 6, 7, and 8), $E = 10^7 kPa$

| 2D cases | $J(\boldsymbol{x}_i^*)$ | Material | | Volume | Final | # |
|---|---|---|---|---|---|---|
| | $(kN \cdot m)$ | $E_t$ | $E_c$ | constraint, $V_{\max}^j$ | $V_{\text{frac}}$ | Elements |
| 1 material | 1.136 | $7E$ | $2E$ | $V_{\max}$ | 1.00 | 48 |
| 2 materials | 1.136 | $7E$ | 0 | $V_{\max}$ | 0.63 | 25 |
| (1 vol. constraint) | | 0 | $2E$ | | 0.37 | 19 |
| 2 materials | 1.179 | $7E$ | 0 | $0.5V_{\max}$ | 0.5 | 42 |
| (2 vol. constraints) | | 0 | $2E$ | $0.5V_{\max}$ | 0.5 | 33 |

the program GRAND3 (Zegard and Paulino 2015). It is worth noting that we do not verify the stability of members. For studies that address stability issues, readers are referred to Rozvany (1996), Achtziger (1999a), Achtziger (1999b), Ben-Tal et al. (2000), and Tyas et al. (2006). The GSM without stability constraints may lead to structures with aligned nodes, i.e., hinges connecting two collinear members. The procedure for removing aligned nodes consists of

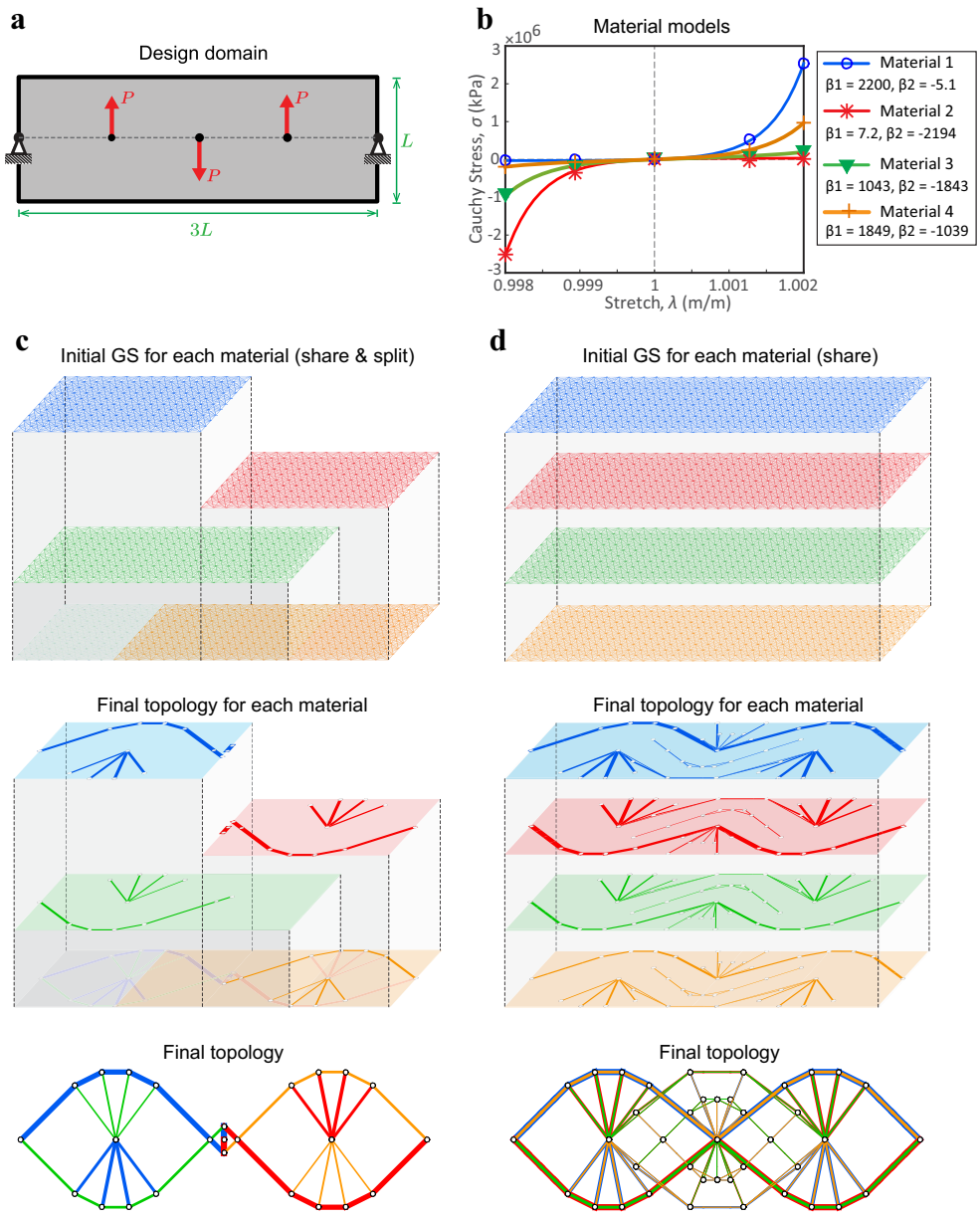


**Fig. 9** Example 2: influence of initial material distributions. **a** Design domain ($L = 10m$, $P = 1000kN$); **b** material models: four Ogden-based materials; **c** initial material distribution (schematic GSs) and the corresponding optimized structure for the case of materials sharing & splitting the domain; **d** initial material distribution (schematic GSs) and the corresponding optimized structure for the case of materials sharing the entire domain. (Online version in color)

**Table 5** Numerical information for Example 2 (Fig. 9)

| 2D cases | $J(\boldsymbol{x}_i^*)$ | Material | | Volume | # |
|---|---|---|---|---|---|
| | $(kN \cdot m)$ | $\beta_1$ | $\beta_2$ | constraint, $V_{\max}^j$ | Elements |
| 4 materials | 35.44 | 2200.3 | −5.1 | $0.4V_{\max}$ | 11 |
| | | 7.2 | −2194.0 | $0.4V_{\max}$ | 11 |
| (share & split) | | 1043.3 | −1843.1 | $0.1V_{\max}$ | 10 |
| | | 1848.8 | −1039.2 | $0.1V_{\max}$ | 10 |
| 4 materials | 27.53 | 2200.3 | −5.1 | $0.4V_{\max}$ | 42 |
| | | 7.2 | −2194.0 | $0.4V_{\max}$ | 42 |
| (share) | | 1043.3 | −1843.1 | $0.1V_{\max}$ | 42 |
| | | 1848.8 | −1039.2 | $0.1V_{\max}$ | 42 |

identifying the nodes that connect only two collinear members (except those nodes connecting to load or displacement boundary conditions). Then we remove the aligned node by replacing two collinear members with one long member that takes the larger (or equal) area from the two. Therefore, the resulting objective value decreases (or remains unchanged). For all GSM results, we remove aligned nodes and floating members and check the final topologies to ensure that they are at global equilibrium. A detailed explanation can be found in the references (Zhang et al. 2016; Zhang et al. 2017). The nonlinear solution scheme is based on a Newton-Raphson approach with line search (see Zhang et al. 2017) for a detailed explanation). For all the examples, the discrete filter is used to obtain valid structures and improve computational efficiency (see Section 2.3). We use the filter value $\alpha_f = 10^{-4}$ during the optimization process, and the filter operation is performed at every optimization step. Consistent units are implied throughout, and all the examples have initial tangent modulus, $E_0 = 7 \times 10^7 kPa$; stopping criterion: $\text{tol}_{\text{opt}} = 10^{-9}$; move value: $move = 10^4 x^0$, where $x^0$ is the initial guess of the design variables; and initial damping factor for the ZPR design update scheme: $\eta = 0.5$. Subsequent damping factors are updated according to the scheme provided by Groenwold and Etman (2008). The upper bound for the design variable is defined by $x_{\max} = 10^4 x^0$. *All of our examples are solved by the ZPR design update scheme proposed in Section 3*. The examples are summarized in Table 3.

### 5.1 Example 1: Verification of the multi-material topology optimization framework

The first example verifies the proposed multi-material methodology and the ZPR design update scheme by comparing

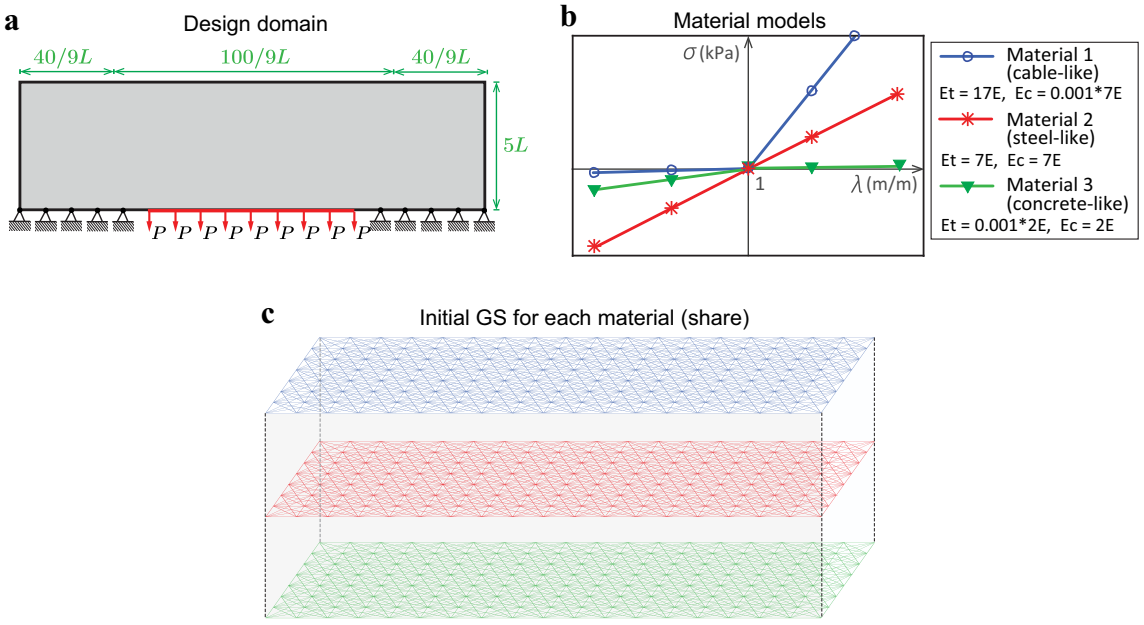


**Fig. 10** Example 3: influence of volume constraint combinations. **a** Design domain ($L = 1m$, $P = 100kN$); **b** material models: two bilinear and one linear materials; **c** initial full-level (schematic) GS for each material. (Online version in color)

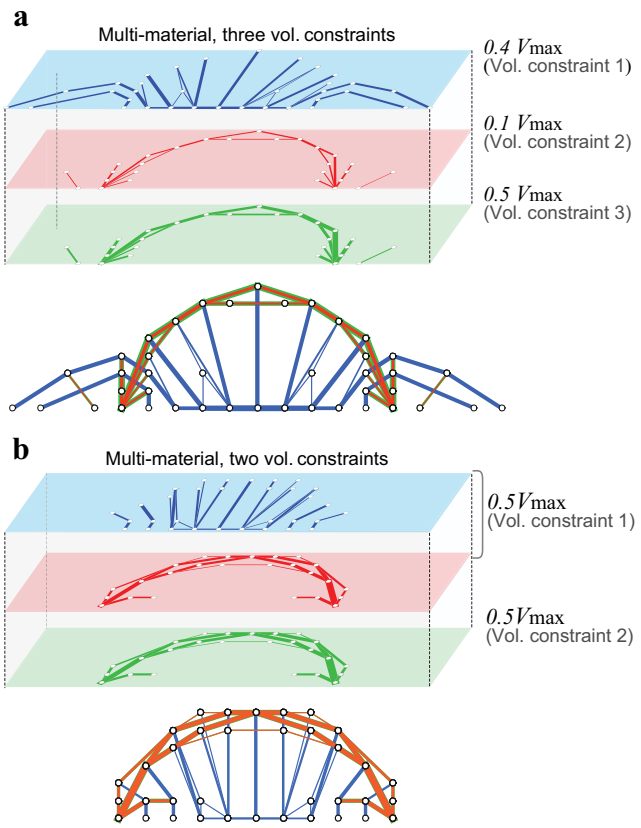


**Fig. 11** Example 3: influence of volume constraint combinations. **a** Optimized structure for the first volume constraint combination (3 constraints) where each material is assigned to an individual constraint; **b** optimized structure for the second volume constraint combination (2 constraints) where cable-like and steel-like materials are assigned to one constraint and the concrete-like material is assigned to another constraint. (Online version in color)

the results obtained from the proposed formulation (using two bilinear materials) with the results obtained from the standard GSM using a single (bilinear) material. We use a 2D box domain, discretized by a $30 \times 10$ grid. The geometry ($L = 10m$), load ($P = 100kN$), and support conditions (two fixed supports) are shown in Fig. 6. The total prescribed maximum volume takes the following value, $V_{\max} = 0.15m^3$.

For the single material case, using a level-10 initial ground structure with 19,632 non-overlapped members and 341 nodes, we perform optimization with a bilinear material ($E_t = 7E$ and $E_c = 2E$, $E = 10^7 kPa$). For the two multi-material cases, two materials share the entire domain. Hence, we use two layers of level-10 initial ground structures (one for each material) with 39,264 members (truss members within each material layer are not overlapped), 341 nodes, and two bilinear materials ($E_{t1} = 7E$, $E_{c1} = 0$ and $E_{t2} = 0$, $E_{c2} = 2E$). The combination of these two materials is designed to reproduce the results from the single material case. For multi-material cases, two scenarios of assignments for volume constraints are used. In one scenario, two materials are assigned to one total volume constraint ($nc = 1$), i.e., $V^1_{\max} = V_{\max}$; in another scenario, each material is assigned to an individual volume constraint ($nc = 2$), i.e., $V^j_{\max} = 0.5V_{\max}$, $j = 1, 2$. Note that in all single and multiple materials cases, the prescribed maximum volume, $V_{\max}$, is the same. The initial ground structures, material models, and optimized structures obtained using one bilinear material and two bilinear materials are shown in Figs. 7 and 8, respectively. The associated numerical information is summarized in Table 4.

The multi-material formulation with one volume constraint (Fig. 8c) yields a structure and an optimal objective value identical to those obtained using the single material formulation (Fig. 7c). This comparison verifies the proposed formulation and the ZPR design update scheme. In addition, for the case that two materials share the entire domain and are assigned to one volume constraint, the optimizer assigns materials to appropriate locations with proper amounts according to each material's property. For the case with two constraints (Fig. 8d), the optimized structure differs from the one volume constraint case (Fig. 8c) and has a slightly (3.7%) higher objective value.

### 5.2 Example 2: Opposite loads in a simply supported rectangular domain

In the second example, we demonstrate the different scenarios of initial material distributions using four Ogden-based materials in the proposed methodology and compare their

**Table 6** Numerical information for Example 3 (Figs. 10, 11, and 12), $E = 10^7 kPa$

| 2D cases | $J(\boldsymbol{x}^*_i)$ | Material | | Volume | Final | # |
|---|---|---|---|---|---|---|
| | $(kN \cdot m)$ | $E_t$ | $E_c$ | constraint, $V^j_{\max}$ | $V_{\text{frac}}$ | Elements |
| 3 materials | 20.957 | $17E$ | $0.001E$ | $0.4V_{\max}$ | 0.40 | 35 |
| | | $7E$ | $7E$ | $0.1V_{\max}$ | 0.10 | 27 |
| (3 vol. constraints) | | $0.002E$ | $2E$ | $0.5V_{\max}$ | 0.50 | 27 |
| 3 materials | 14.755 | $17E$ | $0.001E$ | $0.5V_{\max}$ | 0.16 | 31 |
| | | $7E$ | $7E$ | | 0.34 | 31 |
| (2 vol. constraints) | | $0.002E$ | $2E$ | $0.5V_{\max}$ | 0.50 | 31 |

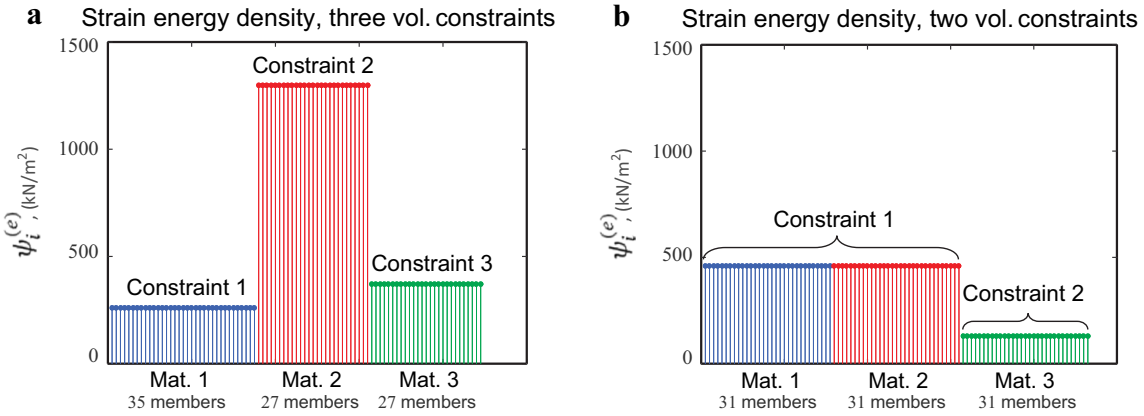


**Fig. 12** Example 3: influence of volume constraint combinations. **a** Strain energy density for the first volume constraint combination (3 constraints); the members within the same volume constraint have identical values of strain energy density. **b** Strain energy density for the second volume constraint combination (2 constraints); the members within the same volume constraint have identical values of strain energy density, regardless of the material type, which verifies the KKT conditions discussed in Section 2.2. (Online version in color)

optimized results. The design domain with load and boundary conditions ($L = 10m, P = 1000kN$) and material models are shown in Fig. 9a and b. We compare two scenarios of initial material distributions. In the first scenario, four materials share & split the domain (Fig. 9c), resulting 55,818 members and 341 nodes. The total prescribed maximum volume takes the following value, $V_{\max} = 0.15m^3$. Each material is associated with an individual volume constraint ($nc = 4$), as shown in Table 5. The initial GS for each material and the corresponding optimized structures are shown in Fig. 9c. The multi-material framework with materials sharing & splitting the domain leads to a structure without overlapping members (selecting at most one material for each subdomain). In the final design without any overlapping members, the values of strain energy density of all the truss members for the same material are identical (Ramos and Paulino 2015; Zhang et al. 2017).

In the second scenario, four materials share the entire domain (Fig. 9d). Four layers (one for each material) of identical level-10 initial ground structures (based on a $30 \times 10$ grid) with a total of 78,528 members and 341 nodes are used. Similar to the first scenario, the total prescribed maximum volume takes the value, $V_{\max} = 0.15m^3$, and each material is associated with an individual volume constraint ($nc = 4$), see Table 5. The initial GSs for the second scenario and the corresponding optimized structures are shown in Fig. 9d. The associated numerical information is summarized in Table 5. In the optimized structure, we observe that the selection of more than one material for some truss members (i.e., overlapping of truss members from different materials) occurs when materials share the entire domain. In this case of selecting more than one material, truss members with several materials may have unequal strain energy density values. While the selection of multiple materials at certain subdomains is beyond the scope of the present work, the results with overlapping members may be realized through composite materials.

### 5.3 Example 3: Long-span bridge design using linear and bilinear materials

This bridge example investigates different combinations of volume constraints using one linear and two bilinear materials in the proposed multi-material formulation. The design domain with load and boundary conditions ($L = 1m, P = 100kN$) is shown in Fig. 10a. Two bilinear and one linear materials are used to represent cable-like ("Material 1"), steel-like ("Material 2"), and concrete-like ("Material 3") materials ($[E_t, E_c]^{\text{cable}} = [17E, 0.007E]$; $[E_t, E_c]^{\text{steel}} = [7E, 7E]$; $[E_t, E_c]^{\text{concrete}} = [0.002E, 2E]$; where $E = 10^7 kPa$), as shown in Fig. 10b. Three materials share the entire domain, as shown in Fig. 10c, leading to three identical layers of full-level initial ground structures (based on an $18 \times 7$ grid) with 21,249 non-overlapping members and 152 nodes. We use two combinations of assignments for volume constraints. In one combination (three volume constraints, $nc = 3$), each material is assigned to an individual volume constraint (Fig. 11a). In the other combination (two volume constraints, $nc = 2$), cable-like and steel-like materials are assigned to one volume constraint, and the concrete-like material is assigned to another volume constraint (Fig. 11b), see Table 6. Note that in both combinations, the prescribed maximum volume, $V_{\max} = 0.05m^3$, is the same. The optimized structures for the two combinations of volume constraints are shown in Fig. 11. The associated numerical information is summarized in Table 6. Different combinations of volume constraints lead to varied optimized structures. The case with two constraints has

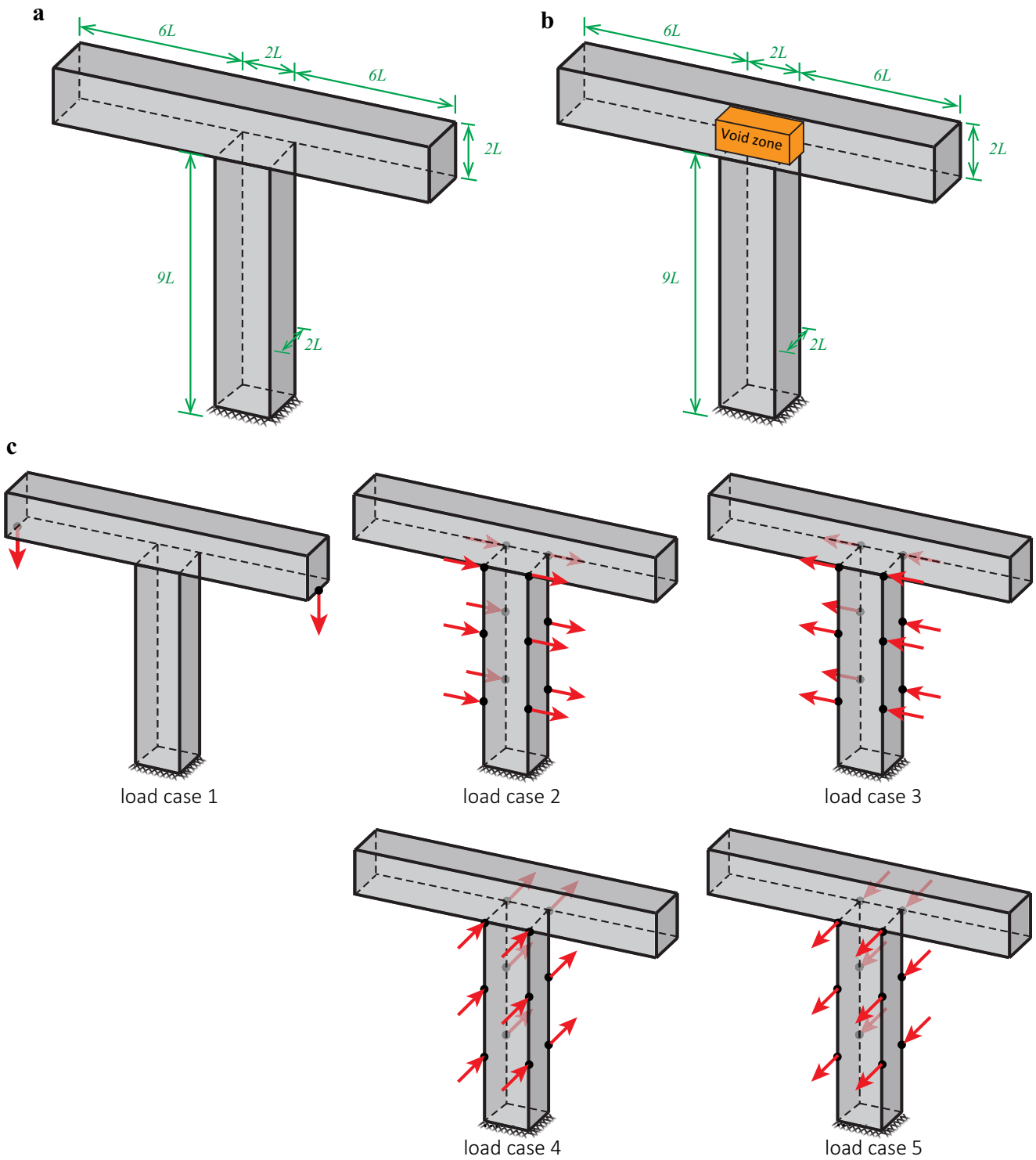


**Fig. 13** Example 4: multi-material crane design with multiple load cases. **a** Design domain discretized using a $14 \times 2 \times 2$ grid for the top domain and a $2 \times 2 \times 10$ grid for the bottom domain; **b** design domain with void zone; **c** five equal-weighted load cases

smaller objective value than the case with individual volume constraint for each material (i.e., three constraints). The amount of usage for the cable-like material decreases when its volume constraint is combined with a steel-like material. The strain energy density for each member in these two combinations of volume constraints are shown in Fig. 12. In

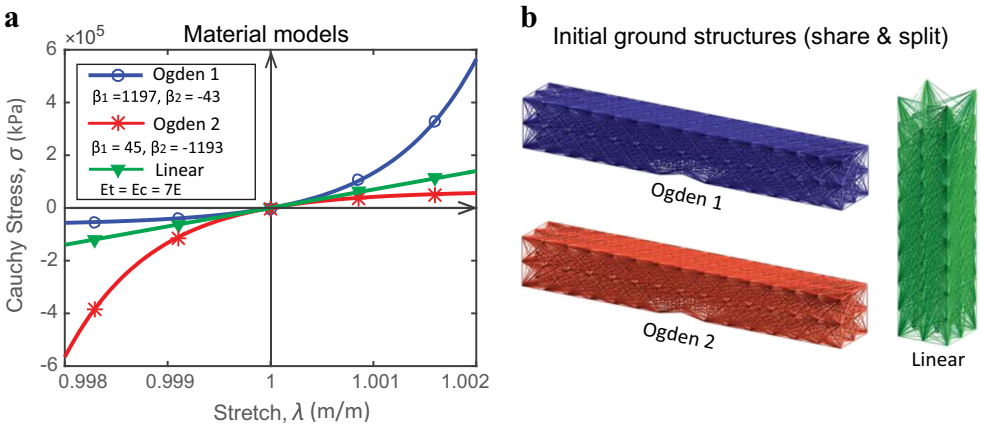


**Fig. 14** Example 4: multi-material crane design with multiple load cases. **a** Material models: two Ogden-based and one linear materials; **b** illustration of the initial material distribution. (Online version in color)

the optimized design, we observe that the members within the same volume constraint have the same strain energy density value regardless of the material type, verifying the KKT conditions discussed in Section 2.2. In the case that "Material 1" and "Material 2" are assigned to one volume constraint, the strain energy density values in the optimized structure are the same even though the properties of the two candidate materials are different.

### 5.4 Example 4: 3D crane design subjected to multiple load cases

Using a combination of different materials with a more general volume constraint setting, we apply the proposed multi-material formulation to a 3D crane design subjected to multiple load cases. These load cases are implemented using the weighted-sum formulation, which averages the

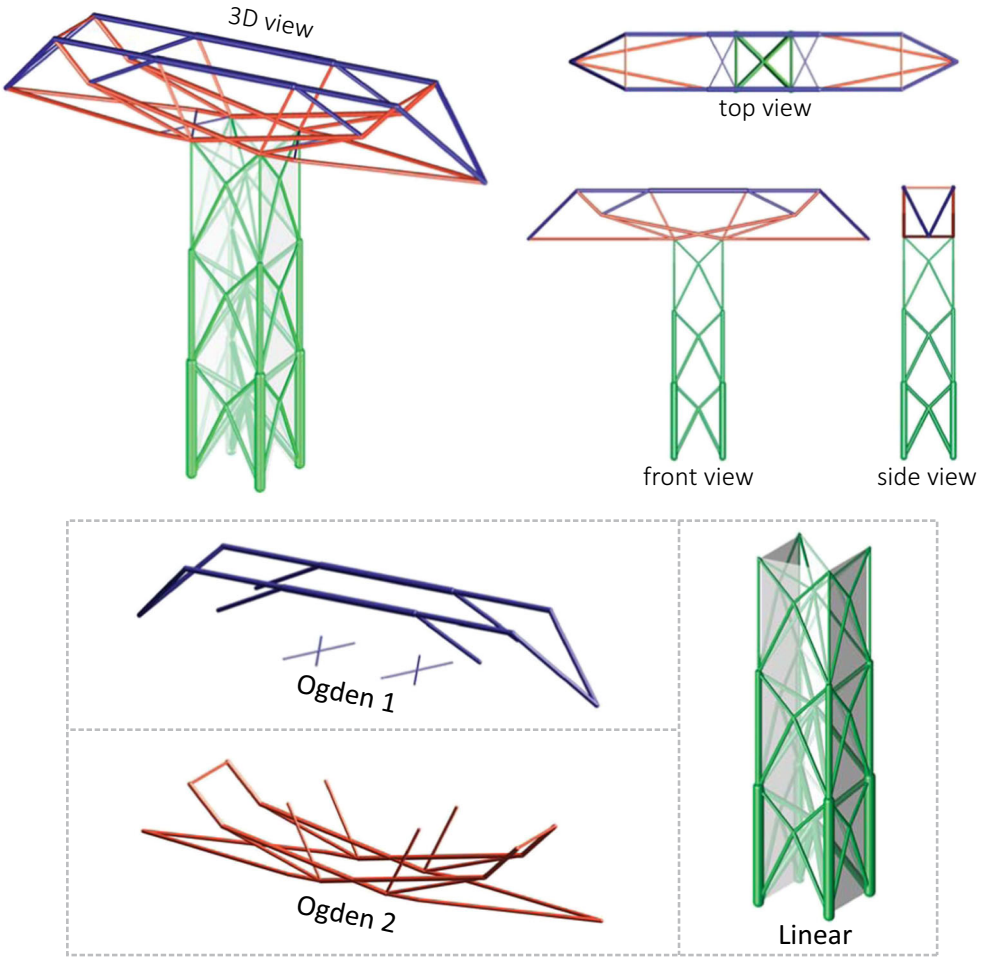


**Fig. 15** Example 4: the optimized structure for the 3D crane design – no overlapping members are observed in the final design. (Online version in color)

**Table 7** Numerical information for Example 4 (Figs. 13, 14, 15, and 16), $E = 10^7 kPa$

| 3D case | $J(\boldsymbol{x}_i^*)$ | Material | | Volume | $V_{\text{frac}}$ | | # |
|---|---|---|---|---|---|---|---|
| | $(kN \cdot m)$ | type | property | constraint, $V_{\max}^j$ | initial | final | Elements |
| 3 mats. | 457 | Ogden | $\beta_1 = 1197, \beta_2 = -43$ | $0.4V_{\max}$ | 0.2 | 0.20 | 18 |
| (share | | Ogden | $\beta_1 = 45, \beta_2 = -1193$ | | 0.2 | 0.20 | 26 |
| & split) | | Linear | $E_T = E_c = 7E$ | $0.6V_{\max}$ | 0.60 | 0.60 | 84 |

objective functions from all load cases. The geometry of the crane ($L = 1m, P = 60kN$), in Fig. 13a and b, has a fixed end and a void zone for practical design purposes (Zegard and Paulino 2015). To obtain constructible structures, we use a $14 \times 2 \times 2$ grid (with a level 6 GS) for the top domain and a $2 \times 2 \times 10$ grid (with a level 3 GS) for the bottom domain, containing a total of 10,276 members and 216 nodes. As shown in Fig. 13c, five equal-weighted load cases are applied to the crane. We perform optimization with three materials (one linear and two Ogden-based materials), as shown in Fig. 14a. As indicated by the initial GSs (Fig. 14b), these three materials share & split the domain, we assign two Ogden-based materials to the top domain and the linear material to the bottom domain.

Two volume constraints are used ($nc = 2$) where two Ogden-based materials are associated with one constraint, and the linear material is associated with the second constraint. The total prescribed maximum volume takes the following value, $V_{\max} = 0.014m^3$. In addition to a small filter ($\alpha_f = 10^{-4}$) used in the entire optimization, we apply a larger filter ($\alpha_f = 10^{-2}$) in the final step of the optimization to control the resolution of the final topology. The optimized structure is shown in Fig. 15. The associated numerical information is summarized in Table 7. The multi-material framework with multiple load cases leads to a crane design with a clear layout and no overlapping members. In fact, the lower part of the crane design exhibits the 2/3 bracing rule (Zegard et al. 2014), which is shown to be the optimal bracing point for lateral loads. The values of initial and final volume fractions of the two Ogden-based materials in Table 7 indicate that the optimizer chooses and distributes the materials according to their properties. The geometry data of this crane design (Fig. 15) is exported to STL (or stereolithography) format using the method proposed by Zegard and Paulino (2016). The design is then manufactured with 3D printing using a fused deposition modeling (FDM) process and painted using multiple colors, each corresponding to one material, as shown in Fig. 16.

## 6 Concluding remarks

In this paper, we propose a general multi-material formulation for truss topology optimization using the GSM considering material nonlinearity. This formulation is designed to handle an arbitrary number of candidate materials. Each candidate material is associated with an individual layer of the ground structure. Therefore, the location of each material layer can be freely specified – multiple material layers can either share or split the design domain, or combine both. For each material, the choice of the constitutive model is flexible and independent. As shown by the KKT conditions

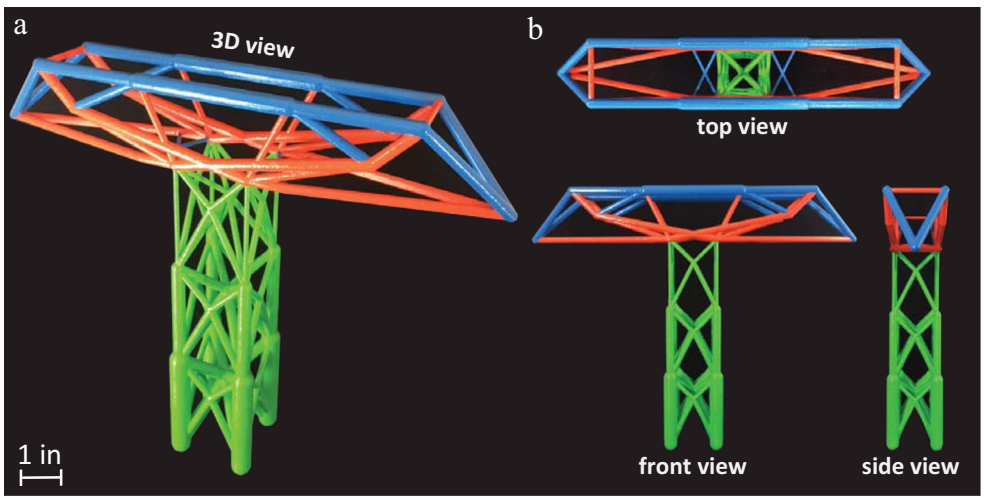


**Fig. 16** Example 4: printed model of the optimized crane design with three materials using FDM process. **a** 3D view; **b** top, front, and side views. The dimension of the manufactured model is 12.8 in × 2.3 in × 10.2 in. (Online version in color)

(see Section 2.2), our formulation leads to identical values of strain energy density for members within the same volume constraint (and whose optimal design variables are in the optimum range $x_{\min} < x_i^{(e),*} < x_{\max}$), regardless of the material type (see (12) and Fig. 12). Furthermore, the assignment of volume constraints is generalized in the proposed formulation (e.g., one volume constraint can be assigned to either one or multiple materials). To efficiently handle the generalization of volume constraints, the ZPR design update scheme is utilized, which performs efficient and robust updates of the design variables associated with each volume constraint independently.

By means of several 2D and 3D examples, using combinations of Ogden-based, bilinear, and linear materials, we verify and demonstrate the effectiveness of the proposed multi-material formulation and the ZPR design update scheme. The incorporation of material nonlinearity is shown to naturally eliminate the tendency of multi-material optimization, using linear materials, to favor the stiffest material. In addition, different initial material distributions are found to provide a variety of optimized structures. In certain scenarios (e.g., the scenario of multiple materials sharing the domain), the selection of more than one material for truss members (the overlapping of truss members from different materials) in the final design may occur, which may denote a composite material configuration. Furthermore, the comparison of different combination of volume constraints shows that fewer constraints on the material volume lead to stiffer optimized structures. In the case of one total/global volume constraint with all materials sharing the entire domain, we achieve automatic assignment of the materials, that is, the optimizer chooses and distributes the materials according to their properties. In this case, the stiffest optimized structures are achieved. Multiple load cases using a combination of various materials and a more general volume constraint assignment are considered in the 3D crane design. The multi-material framework with multiple load cases leads to a crane design exhibiting the 2/3 bracing rule (Zegard et al. 2014), which has been shown to be the optimal bracing point for lateral loads. The optimized crane was manufactured with 3D printing (using FDM) and painted using multiple colors that are consistent with the material assignment scheme.

Given the present investigation and outcome of the examples, we conclude that the proposed multi-material topology optimization framework, which accounts for material nonlinearity using the ZPR update scheme, leads to a design tool that not only finds the optimal topology but also selects the proper type and the amount of material. The ZPR design update scheme is flexible and customized to handle a general number of volume constraints – it is also applicable to continuum topology optimization with multiple volume constraints.

This work provides insights for future multi-material topology optimization research. One possible direction is the extension of the present framework to large-scale parallel computing in both the structural and the optimization models. For multiple load cases, each load case can be done in parallel (e.g., displacement and sensitivity), and the update of the Lagrange multipliers and design variables in the ZPR update scheme can also be done in parallel for each volume constraint. Another direction is to enforce the selection of at most one type of material at each design subdomain in the final design to eliminate overlapping members. In addition, multi-material formulations can be applied to the design of lattice structures. Finally, the connection of multi-material topology optimization to additive manufacturing should be further explored.

**Acknowledgements** The authors acknowledge the financial support from the US National Science Foundation (NSF) under projects #1559594 (formerly #1335160) and #1321661, from the Brazilian agency CNPq (National Council for Research and Development), and from the Laboratory of Scientific Computing and Visualization (LCCV) at the Federal University of Alagoas (UFAL). We are also grateful for the endowment provided by the Raymond Allen Jones Chair at the Georgia Institute of Technology. The information provided in this paper is the sole opinion of the authors and does not necessarily reflect the views of the sponsoring agencies.

## Appendix: Nomenclature

| | |
|---|---|
| $\alpha$ | Exponent coefficient used in the ZPR model to define $\boldsymbol{y}_i$ |
| $\alpha_f$ | Filter value |
| $\eta$ | Damping factor in the ZPR model |
| $\Gamma$ | Tikhonov regularization parameter |
| $\gamma_i$, $\beta_i$ | Ogden material parameters |
| $\lambda$ | Linearized stretch |
| $\Lambda$, $\mu$ | Lamé constants |
| $\lambda_i$ | Principal stretches |
| $\mathscr{G}^j$ | The set of material indices associated with the $j$th volume constraint in the ZPR model |
| $\overline{\boldsymbol{x}}_i$ | Vector of filtered design variables (cross-sectional areas) with material $i$ |
| $\overline{x}_i^{(e)}$ | Filtered cross-sectional area of member $e$ with material $i$ |
| $\phi_V^j$ | Lagrange multiplier introduced for the $j$th volume constraint in the ZPR model |
| $\phi_V^{j*}$ | The optimal Lagrange multiplier introduced for the $j$th volume constraint in the dual problem of the ZPR model |
| $\Pi$ | Total potential energy |
| $\Psi_i^{(e)}$ | Strain energy density function of member $e$ with material $i$ |
| $\Psi_{Bi}$ | Bilinear strain energy density function |

| | |
|---|---|
| $\Psi_{OG}$ | Ogden strain energy density function |
| $\sigma$ | Principal Cauchy stress |
| $\boldsymbol{b}_i(\boldsymbol{x}_1^k, ..., \boldsymbol{x}_m^k)$ | Sensitivity vector of the objective function $J$ with respect to $\boldsymbol{y}_i$ evaluated at the $k$th step in the ZPR model |
| $\boldsymbol{f}$ | External force vector |
| $\boldsymbol{L}_i$ | Vector of member length for material $i$ |
| $\boldsymbol{N}$ | Unit directional vector of a given truss member |
| $\boldsymbol{u}$ | Displacement vector |
| $\boldsymbol{u}_p, \boldsymbol{u}_q$ | Displacements of nodes $p$ and $q$ for a given truss member |
| $\boldsymbol{x}_i$ | Vector of design variables (cross-sectional areas) with material $i$ |
| $\boldsymbol{y}_i$ | Vector of intervening variables with material $i$ |
| $d$ | Number of dimensions (e.g., $d = 2, 3$) |
| $E_0$ | Initial tangent modulus (Young's modulus) |
| $E_T$ | Tangent modulus |
| $g^j$ | The $j$th volume constraint in the ZPR model |
| $J$ | Objective function |
| $J^k$ | Approximated objective function in the subproblem at optimization step $k$ |
| $L_i^{(e)}$ | Length of truss member $e$ with material $i$ |
| $M$ | Ogden material parameter |
| $m$ | Total number of materials |
| $M_i$ | Number of truss members in material $i$ |
| $move$ | Prescribed move limit in the ZPR model |
| $nc$ | Total number of volume constraints in the ZPR model |
| $\text{tol}_{\text{opt}}$ | Tolerance value |
| $V_{\max}^j$ | Prescribed maximum volume in the $j$th volume constraint of the ZPR model |
| $x_{\max}$ | Upper bound for design variables |
| $x_{\min}$ | Lower bound for design variables |
| $x_i^{(e)}$ | Cross-sectional area of member $e$ with material $i$ |
| $x_{i,L}^{(e),k}$ | The lower bound of the $e$th design variable with material $i$ in the subproblem at optimization step $k$ in the ZPR model |
| $x_{i,U}^{(e),k}$ | The upper bound of the $e$th design variable with material $i$ in the subproblem at optimization step $k$ in the ZPR model |

## References


Achtziger W (1996) Truss topology optimization including bar properties different for tension and compression. Struct Optim 12(1): 63–74

Achtziger W (1999a) Local stability of trusses in the context of topology optimization part i: Exact modelling. Struct Multidiscip Optim 17(4):235–246

Achtziger W (1999b) Local stability of trusses in the context of topology optimization part II: a numerical approach. Struct Optim 17(4):247–258

Amir O, Sigmund O (2013) Reinforcement layout design for concrete structures based on continuum damage and truss topology optimization. Struct Multidiscip Optim 47(2):157–174

Ben-Tal A, Jarre F, Kočvara M, Nemirovski A, Zowe J (2000) Optimal design of trusses under a nonconvex global buckling constraint. Optim Eng 1(2):189–213

Bendsøe MP, Sigmund O (1999) Material interpolation schemes in topology optimization. Arch Appl Mech 69(9-10):635–654

Bendsøe MP, Sigmund O (2003) Topology optimization: theory, methods, and applications. Springer, Berlin

Bogomolny M, Amir O (2012) Conceptual design of reinforced concrete structures using topology optimization with elastoplastic material modeling. Int J Numer Methods Eng 90(13):1578–1597

Bonet J, Wood RD (2008) Nonlinear continuum mechanics for finite element analysis. Cambridge University Press

Christensen P, Klarbring A (2009) An introduction to structural optimization. Springer Science & Business Media, Linköping

Cui M, Chen H (2014) An improved alternating active-phase algorithm for multi-material topology optimization problems. In: Applied mechanics and materials, Trans Tech Publ, vol 635, pp 105–111

Dorn WS, Gomory RE, Greenberg HJ (1964) Automatic design of optimal structures. J de Mecanique 3:25–52

Felippa C (n.d) Newton method: General control and variants. Lecture notes. http://www.colorado.edu/engineering/cas/courses.d/NFEM.d/NFEM.ch26.d/NFEM.ch26.pdf

Gaynor A, Guest J, Moen C (2012) Reinforced concrete force visualization and design using bilinear truss-continuum topology optimization. J Struct Eng 139(4):607–618

Gibiansky LV, Sigmund O (2000) Multiphase composites with extremal bulk modulus. J Mech Phys Solids 48(3):461–498

Groenwold AA, Etman LFP (2008) On the equivalence of optimality criterion and sequential approximate optimization methods in the classical topology layout problem. Int J Numer Methods Eng 73(3):297–316

Haftka RT, Gürdal Z (1992) Elements of structural optimization. Springer, Netherlands

Hvejsel CF, Lund E (2011) Material interpolation schemes for unified topology and multi-material optimization. Struct Multidiscip Optim 43(6):811–825

Kirsch U (1989) Optimal topologies of truss structures. Comput Methods Appl Mech Eng 72(1):15–28

Kirsch U (1993) Structural optimization: fundamentals and applications. Springer, Berlin

Klarbring A, Rönnqvist M (1995) Nested approach to structural optimization in nonsmooth mechanics. Struct Optim 10(2):79–86

Mei Y, Wang X (2004) A level set method for structural topology optimization with multi-constraints and multi-materials. Acta Mech Sinica 20(5):507–518

Ogden RW (1984) Non-linear elastic deformations. Dover Publications Inc, Mineola

Ohsaki M (2010) Optimization of finite dimensional structures. CRC Press, Boca Raton

Park J, Sutradhar A (2015) A multi-resolution method for 3D multi-material topology optimization. Comput Methods Appl Mech Eng 285:571–586

Ramos AS Jr, Paulino GH (2015) Convex topology optimization for hyperelastic trusses based on the ground-structure approach. Struct Multidiscip Optim 51(2):287–304

Ramos AS Jr, Paulino GH (2016) Filtering structures out of ground structures – a discrete filtering tool for structural design optimization. Struct Multidiscip Optim 54(1):95–116

Rozvany GIN (1996) Difficulties in truss topology optimization with stress, local buckling and system stability constraints. Struct Optim 11(3):213–217

Rozvany GIN, Bendsoe MP, Kirsch U (1995) Layout optimization of structures. Appl Mech Rev 48(2):41–119

Sigmund O, Torquato S (1997) Design of materials with extreme thermal expansion using a three-phase topology optimization method. J Mech Phys Solids 45(6):1037–1067

Sokół T (2011) A 99 line code for discretized Michell truss optimization written in Mathematica. Struct Multidiscip Optim 43(2): 181–190

Stanković T, Mueller J, Egan P, Shea K (2015) A generalized optimality criteria method for optimization of additively manufactured multimaterial lattice structures. J Mech Des 137(11):111,405–1

Stegmann J, Lund E (2005) Discrete material optimization of general composite shell structures. Int J Numer Methods Eng 62(14):2009–2027

Stolpe M, Svanberg K (2001) An alternative interpolation scheme for minimum compliance topology optimization. Struct Multidiscip Optim 22(2):116–124

Svanberg K (1987) The method of moving asymptotes – a new method for structural optimization. Int J Numer Methods Eng 24(2): 359–373

Talischi C, Paulino GH (2013) An operator splitting algorithm for Tikhonov-regularized topology optimization. Comput Methods Appl Mech Eng 253:599–608

Tavakoli R, Mohseni SM (2014) Alternating active-phase algorithm for multimaterial topology optimization problems: a 115-line matlab implementation. Struct Multidiscip Optim 49(4):621–642

Tikhonov A, Arsenin V (1977) Methods for solving ill-posed problems. Wiley, New York

Tyas A, Gilbert M, Pritchard T (2006) Practical plastic layout optimization of trusses incorporating stability considerations. Comput Struct 84(3C4):115–126

Victoria M, Querin OM, Martí P (2011) Generation of strut-and-tie models by topology design using different material properties in tension and compression. Struct Multidiscip Optim 44(2): 247–258

Wallin M, Ivarsson N, Ristinmaa M (2015) Large strain phase-field-based multi-material topology optimization. Int J Numer Methods Eng 104(9):887–904

Wang MY, Wang X (2004) Color level sets: a multi-phase method for structural topology optimization with multiple materials. Comput Methods Appl Mech Eng 193(6):469–496

Wang MY, Wang X (2005) A level-set based variational method for design and optimization of heterogeneous objects. Comput Aided Des 37(3):321–337

Wang MY, Chen S, Wang X, Mei Y (2005) Design of multimaterial compliant mechanisms using level-set methods. J Mech Des 127(5):941–956

Yin L, Ananthasuresh G (2001) Topology optimization of compliant mechanisms with multiple materials using a peak function material interpolation scheme. Struct Multidiscip Optim 23(1):49–62

Yin L, Yang W (2001) Optimality criteria method for topology optimization under multiple constraints. Comput Struct 79(20):1839–1850

Zegard T, Paulino GH (2013) Truss layout optimization within a continuum. Struct Multidiscip Optim 48(1):1–16

Zegard T, Paulino GH (2014) GRAND – Ground Structure based topology optimization for arbitrary 2D domains using MATLAB. Struct Multidiscip Optim 50(5):861–882

Zegard T, Paulino GH (2015) GRAND3 – Ground Structure based topology optimization for arbitrary 3D domains using MATLAB. Struct Multidiscip Optim 52(6):1161–1184

Zegard T, Paulino GH (2016) Bridging topology optimization and additive manufacturing. Struct Multidiscip Optim 53(1):175–192

Zegard T, William F, Baker F, Mazurek A, Paulino GH (2014) Geometrical aspects of lateral bracing systems: Where should the optimal bracing point be? ASCE J Struct Eng 140(9):04014,063–1–9

Zhang X, Maheshwari S, Ramos AS Jr, Paulino GH (2016) Macroelement and macropatch approaches to structural topology optimization using the ground structure method. ASCE J Struct Eng 142(11):04016,090–1–14

Zhang X, Ramos AS Jr, Paulino GH (2017) Material nonlinear topology design using the ground structure method with a discrete filter scheme. Struct Multidiscip Optim 55(6):2045–2072

Zhou S, Wang MY (2007) Multimaterial structural topology optimization with a generalized cahn–Hilliard model of multiphase transition. Struct Multidiscip Optim 33(2):89–111